

UC Santa Cruz

UC Santa Cruz Electronic Theses and Dissertations

Title

AI Applications to Load Monitoring and Fault Detection for Power Electronics Systems in DC Microgrids

Permalink

<https://escholarship.org/uc/item/5wz9q37s>

Author

Ma, Yue

Publication Date

2022

Peer reviewed|Thesis/dissertation

UNIVERSITY OF CALIFORNIA

SANTA CRUZ

**AI APPLICATIONS TO LOAD MONITORING AND FAULT
DETECTION FOR POWER ELECTRONICS SYSTEMS IN DC
MICROGRIDS**

A dissertation submitted in partial satisfaction

of the requirements for the degree of

DOCTOR OF PHILOSOPHY

in

ELECTRICAL ENGINEERING

by

Yue Ma

June 2022

The Dissertation of Yue Ma is approved:

Professor Leila Parsa, chair

Professor Keith Corzine

Professor Yu Zhang

Peter Biehl
Vice Provost and Dean of Graduate Studies

Copyright © 2022 by Yue Ma
All rights reserved.

Table of Contents	iii
List of Figures	v
List of Tables.....	vii
Abstract	viii
Acknowledgments.....	ix
1. Introduction	1
2. Literature Review.....	5
2.1. Feature Extraction	5
2.2. Classification Monitoring.....	11
2.3. Fault Identification.....	15
3. STFT-LSTM Autoencoder based Deep Learning Approach.....	18
3.1. Fourier Transform Data Driven Deep Learning Approach.....	18
3.1.1. Autoencoder with Long Short-Term Memory Layers	18
3.1.2. Network Training	20
3.1.3. Fourier Transform Feature Extraction	21
3.1.4. Load Monitoring Algorithm.....	23
3.2. Electric Ship System and Potential Fault Description	25
3.2.1. Pulsed Power Load.....	26
3.2.2. Fixed Impedance Load.....	28
3.2.3. Propulsion Motor Drive Load	29
3.3. Verification.....	29
3.3.1. Current Waveform Classification	29
3.3.2. Fault Identification.....	31
3.4. Conclusions	35
4. Wavelet Transform Data-Driven Clustering based Machine Learning Approach	36
4.1. Machine Learning Based Fault Detection and Load Monitoring.....	37
4.1.1. Feature Extraction	38
4.1.2. Event Detection.....	43
4.1.3. Database Training	43
4.1.4. Classification Monitoring.....	44
4.1.5. Shunt Fault Detection.....	45
4.1.6. Arc Fault Detection.....	46
4.2. Simulation Results	48
4.2.1. Naval Shipboard Dc Pulsating Loads	48

4.2.2.	Coil Gun with Shunt Fault and IGBT Gate Fault.....	49
4.2.3.	Fixed Impedance with Series Arcing Fault	51
4.3.	Real-time DSP Implementation.....	53
4.4.	Experimental Results.....	55
4.4.1.	Coil Gun with Shunt Fault and IGBT Gate Fault.....	55
4.4.2.	Fixed Impedance with Series Arcing Fault	56
4.5.	Conclusions	57
5.	Contributions and Future Works	58
	Bibliography.....	60

LIST OF FIGURES

Figure 1. Future naval advanced powetechnologies.....	2
Figure 2. LSTM layer architecture.....	18
Figure 3. LSTM cell node.....	19
Figure 4. Autoencoder.	19
Figure 5. Two consecutive windows.....	22
Figure 6. Block diagram for recursive DFT.....	22
Figure 7. Deep learning based load monitoring.....	23
Figure 8. Fault identification system.....	25
Figure 9. Circuit schematic of dc busbar with electric-ship load hardware prototypes.....	27
Figure 10. LSTM RNN classification performance of coil gun (a) and propulsion motor drive (b)	30
Figure 11. Original and reconstructed signals of shunt fault (a), IGBT gate fault (b), arcing fault (c) and partial blocked rotor fault (d)....	33
Figure 12. Three-stage DWT implementation [102]....	39
Figure 13. Three-stage SWT implementation [103]... ..	39
Figure 14. The recursive 5/3 filters for forward wavelet transform [104].....	40
Figure 15. Flow diagram of data-driven machine learning based fault detection and load monitoring algorithm....	47
Figure 16. Naval pulsed-power load hardware prototype. (a) Coil gun pulsed-power load and (b) fixed impedance load.....	48
Figure 17. Circuit schematic of pulse load hardware prototypes.....	49
Figure 18. Simulation result of coil-gun load with shunt fault.....	51
Figure 19. Simulation result of coil-gun load with IGBT faul.....	52
Figure 20. Simulation result of fixed impedance load with series arcing fault.....	53

Figure 21. Real-time experimental result of fourteen load cycles with normal and faulty operations of the coil gun.55

Figure 22. Real-time experiment result of eleven load cycles with normal and faulty operations of the fixed load.....56

LIST OF TABLES

TABLE I. Hardware Parameters..	26
TABLE II. Identification Confusion Matrix.....	32
TABLE III. Existing Methods Comperision.....	40
TABLE IV. Hardware Design Parameters.....	49
TABLE V. Detection Parameters and Performance Summary of Simulation and Experimental Results.....	54

ABSTRACT

AI Applications to Load Monitoring and Fault Detection for Power Electronics Systems in DC Microgrids

Yue Ma

Extensive deployment of power electronic loads in naval ship power systems indicate full ship electrification is inevitable. Next generation warships require high power density weapons drawing pulse power from a dc power grid. A particularly concerning issue is that these pulse loads draw large currents in short periods of time and are similar in behavior to a fault; and therefore may be indiscernible from a fault. This dissertation introduces novel machine/deep learning based algorithms, including long short-term memory recurrent neural network based autoencoders and data-driven clustering based machine learning approaches to detect dc faults and monitor load conditions applied to naval pulse loads. Two feature extraction methods are also implemented including the short-time Fourier transform and stationary wavelet transform. The novel load monitoring solution presented herein can be applied to any load profile that exhibits repetitive transients during normal operation. The frequency-domain features of the load current are extracted for the network training to set the network weights and biases. Once the network training is completed, the machine/deep learning approach will predict both signal classification and fault identification. Finally, the method is demonstrated in a low power laboratory system meant to mimic naval shipboard power systems.

ACKNOWLEDGMENTS

First of all, I would like to express my deepest appreciation to my advisor, Dr. Keith Corzine, for his guidance and support. During my Ph.D. studies, he showed me how to do good research independently with his profound knowledge, wisdom, and patience. He always gave me enough freedom and encouragement to explore the potential research topics. Also, I learned about how to better work and communicate with other people, which will benefit my future career life.

I am also deeply grateful to Dr. Leila Parsa as my committee chair, Dr. Yu Zhang and Dr. Raquel Prado as my committee members for giving generous and valuable suggestions in my research project and disseration.

I would like to thank Dr. Atif Maqsood and Dr. Damian Oslebo, their great personal qualities like patience, calmness, tenderness and logical thinking inspired me on solving technical problems and being a better researcher.

Last but not least, I would like to express my greatest thanks to my parents for their unconditional love and encouragement. I am fearless to overcome challenges and difficulties with you standing behind me.

1.INTRODUCTION

Traditionally, the design of propulsion and electric plant systems are treated separately on United States Navy ships [1]. Future Naval advanced weapon and sensor loads require high power density power electronic distribution systems (PEDS) to be viable. The mission defined electronic loads such as advanced radar and pulsed-power weapons tend to have an irregular power draw and consume a significant amount of power, and would require significant additional generation equipment well beyond the existing power system. The legacy low-voltage ac power grid on a destroyer is already at capacity and since space is at premium, it is unlikely that any new power hungry pulse load could be included without a significant paradigm shift. Further, most of the potential power within the vessel is locked to the mechanical drive system and not readily usable as electrical power. As such, the all-electric ship is the intended option to unlock the mechanical power for various high power pulse loads.

Medium-voltage dc (MVDC) distribution systems provide the energy density to drive these demanding loads. The dual-fed zonal power system has been implemented in Naval warships using the dc distribution systems [2]. Power electronics loads offer unique advantages over traditional loads such as higher efficiency, less weight and volume etc. [3], [4]. It also generates new problems such as stability issue. The Naval vessels feature a host of new technologies for the power architecture as outlined in Figure 1. High-speed generators are need for reduced size

and work well in conjunction the MVDC PEDS. Wide band-gap power conversion systems (WPCS) will serve as an interface to the MVDC backbone and make practical the needed power conversion with limited volume and power losses. Command, control, computers, and communication (C4) provide distributed sensor information and the possibility of alternate control for each power conversion module and improve the survivability.

A particular concern though is that power transient demand of the high-power loads can be misclassified as a fault with traditional protection schemes. To add to this concern, dc faults are potentially more severe than their ac counterparts because

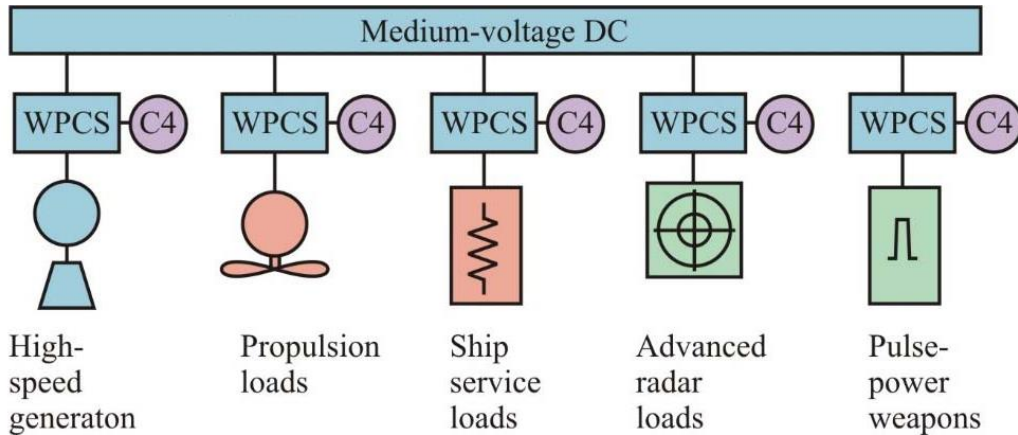


Figure 1. Future naval advanced power technologies.

energy is added continuously to the event without zero crossings in the power delivery that mitigate the full impact. Current circuit protection methods usually assume constant power loads (CPLs) to simplify line impedance measurements for fault identification and converter control. This is because the converter controllers

operate on bandwidths many orders of magnitude larger than that of typical load transients. However, this assumption is not adequate to distinguish pulsed loads from faults, since some high-power pulse transients can complete within milliseconds. Therefore the fault identification and load monitoring scheme is key to the success of MVDC technology.

The requirement for load monitoring would be the identification and classification of pulsed load transient events and to detect anomalous operating behavior on the distribution bus. It is also required to achieve fast enough monitoring performance of the signal bandwidth of the transients. A classification algorithm that takes seconds or more to finish computation, when a typical transient completes on the scale of milliseconds, will not be effective at mitigating fault damage at high voltage potentials. The heat dissipated during open air arc faults presents a significant fire hazard.

Machine learning and Deep learning neural networks can be pipelined to allow for faster sample rates with additional cost to latency. This tradeoff should be balanced by system engineers in the relevant environment to create a load monitoring product with the correct fidelity to properly distinguish pulsed loads from faults but respond fast enough to prevent catastrophic damage.

In machine learning or deep learning neural networks, the first step is feature extraction/event detection such as wavelet transform and Fourier transform [5], in

which certain attributes about the load profile characteristics in pre-defined events are detected and extracted. They are saved one-by-one into the database for the network training process that can be used in the following classification step to identify or label the observed load profile. In this step, the well-trained database is used to identify the feature vector of the detected event. The feature vector input should be similar to other signal types for which the classifier has knowledge in its database. Faults are detected when the classifier cannot easily identify the event.

2. LITERATURE REVIEW

2.1.Feature Extraction

Most of the research on signal feature extraction is focused on ac grid and ac loads with few notable exceptions. Therefore, some of the discussion here will include concepts like harmonics, reactive power and power factor that are primarily concerned with ac loads. Nevertheless, the work summarized here is still relevant because the signal processing techniques to obtain these features are similar to what will eventually be utilized in this project.

Non-intrusive load monitoring (NILM) techniques have long been used in residential power systems to accurately determine energy use [6], [7], [8]. These techniques are typically based on extracting transient-state features but can also involve time-frequency analysis such as the wavelet transform [6]. A number of research publications focus on shipboard power system applications of non-intrusive load monitoring where time-frequency methods are followed by load disaggregation [9], [10], [11]. Load monitoring equipment has been placed on ships, and one valuable outcome has been the ability to determine long-term degradation of components via the load behavior [11], [12]. As an example, a pump that operates at an unusual frequency may indicate a problem with the pump or associated sensors. Unusual spectral components from NILM can be used as triggers to investigate running equipment to conduct early preventative maintenance, rather than corrective maintenance after equipment failure.

A comprehensive look at NILM research shows two broad categories of features exploited for load recognition: macroscopic and microscopic. According to [13] macroscopic features are those extracted at lower sampling frequency, nominally less than 200 Hz, while microscopic features are extracted from data sampled at a higher rate, typically 1kHz and above. Examples of macroscopic features include changes in real and reactive powers, power factors, steady-state RMS values, and the shape and duration of transient events. Common microscopic features are harmonic content of the signal, (extracted through either an FFT or short-time Fourier transform (STFT)), total harmonic distortion (THD), spectral envelope extracted through STFT, wavelet transform coefficients, and high frequency shape features of the raw data.

G.W. Hart pioneered the field of NILM in [14] by using the change in steady-state real and reactive power as the unique identifying feature of the load. This approach worked for large loads with ON/OFF modes and distinct power ratings as one would expect from household appliances. Low power loads or loads with variable or multi-level power draw cannot be identified using this feature only.

Some works have tried to extract more macroscopic features in order to target a wider range of loads. Significant works in this category include the work by A. Cole and A. Albicki [15], [16]. The additional feature they included was the edge count for a given power profile and the variations in real and reactive power over an

extended period of time as long as 900 seconds. In this way they were able to distinguish appliances that had more than one mode of operation and went through several real and reactive power cycles through their operation.

It was later noted that most appliances either have very low reactive power or a prominent real power component, and could be classified based on just the changes in real power alone. This approach is often coupled with features related to the usage pattern of the loads [17], [18]. The earliest work in this area was done by J.T. Powers et al. who used the time of occurrence and frequency of occurrence over a long period as a feature of the load profile [19]. Similarly, the work by Barnaski and Voss extracted features such as duration of use and frequency of change in power levels [20], [21], [22]. Baranski had good success detecting appliances such as refrigerators, heaters, or stoves that have a regular pattern of use. This method requires data storage for five to ten days to reliably look for patterns.

A well-developed load monitoring system based on just macroscopic features is presented in [23]. The program called recognition of electrical appliances and profiling in real time (RECAP), gathers some macroscopic features from the voltage and current data into something called the appliance signature. These features include change in real power, power factor, RMS current, peak voltage, peak current, and signature length. Very similar to this approach is another work presented in [24] which uses power factor and time to reach steady-state power as

additional features, but it is still in the experimental stage so its effectiveness is not known.

In household appliance monitoring applications, fast detection has not been a primary concern so most algorithms using macroscopic features alone perform adequately for their purpose. In some cases, it is easier to differentiate between loads based on microscopic features such as its harmonic content which requires a high sampling frequency. The first work to include harmonics analysis as a feature was done by Sultanem in late 1980s and early 1990s, although he concluded that most household devices could be identified just on the basis of real and reactive power changes [25].

The use of high sampling frequency and microscopic features was developed by Leeb and Shaw at MIT. Leeb's contribution was to extract useful frequency features from turn on transients of various devices rather than steady-state features like changes in power and RMS current [26], [27], [28]. He employed the technique of short-time Fourier transforms (STFT) to calculate the spectral envelope of the signal [27], [28]. Changes in envelope of third and fifth harmonics were monitored over time and recorded as a feature of the transient. A large library of these unique transient features has been developed for a variety of common ac loads and even some dc loads [29], [30], [31], [32]. This form of a load monitoring system has been tested extensively on household and commercial ac loads and recently on U.S Coast

Guard Cutters Spencer (WMEC-905) and Escanaba (WMEC-907), where it has shown promising results and was able to detect deviation from normal behavior in case of worn out equipment [11], [29], [33], [34]. With Shaw's work the focus of NILM has shifted more towards diagnostics [35], [36] along with monitoring of loads but fast fault identification for dc loads has not yet been produced. Following Leeb's work many other research groups have also exploited harmonic content of the transient extracted through STFT as a unique feature of the load [37], [38], [39], [40].

The application of STFT imposes certain limitations on the analysis of the input waveform. The window size of data considered, number of discrete points in the data, and sampling frequency are all fixed which means that the frequency resolution and the range of frequencies analyzed are fixed too. This may limit the ability to detect features from a wide variety of loads. A more advanced harmonic analysis technique called wavelet transform is employed in more recent research that allows the program to zoom into the sampled window of data and retrieve information at various frequency resolutions. The wavelet transform was demonstrated to have an advantage over the STFT when trying to extract frequency information from a transient in [55]. The wavelet transform is usually implemented for real-time application using the discrete time wavelet transform (DWT). In this approach the input data set is passed through a series of high-pass and low-pass filters in a multiresolution analysis (MRA) approach to extract coefficients corresponding to

the energy in various bands of frequencies at various resolutions. After passing through the filter stages the input to the next stage is dyadically (2^N) reduced to ensure the output is the same size as the original signal. Many works recently have used DWT instead of STFT to extract time-frequency features from the input data due to easy access to high speed multicore processors [41], [42], [43], [44], [45], [46], [47], [48], [49].

The stationary wavelet transform (SWT) is a variant to the DWT where the filter stages are dyadically upsampled instead [50]. The key benefit to this approach allows the transient signal response to be the same wherever the transient occurs in the sample window. In the DWT case, a transient response in the beginning of sample window could have a different response than one occurring at the middle or end of the window. The SWT can also be implemented in real-time but requires more system memory to store each of the filter responses at the same size of the original input signal.

Not all microscopic features have to be frequency-based like in the case of STFT or DWT/SWT. Some work has been done on saving high frequency sampled data from raw current and voltage waveform as a way to save the unique signature of every load. The most detailed work in this category is done by Lam et al. where instantaneous voltage and current data (VI) is used to create features to capture the trajectory of each load [51]. These features include direction of the VI trajectory, the

area enclosed by VI over time, measure of asymmetry in the VI trajectory, its curvature, and its slope with reference to the mean value across different segments. Other efforts in the time-domain analysis as a form of feature extraction include [52], [53], [54], [55], [56]. Even better performance is obtained by using a combination of time-domain microscopic characteristics along with frequency-domain features [57], [58]. Using time-domain features reduces the complexity of the feature extraction process, but it is less reliable as some load transients look similar in the time-domain. Furthermore, frequency-based features are more robust to noise and errors in data acquisition [52].

In the presence of so many features that can be used to uniquely identify a load or a transient, the challenge is to pick the right number of features that can reliably identify a reasonable range of common profiles without making the process overly complex and resource-consuming. A notable effort in combining the features to come with the most reliable monitoring system using least number of features is presented in [59].

2.2. Classification Monitoring

The Viterbi algorithm is a commonly used dynamic programming algorithm that recursively solves for a hidden layer of sequence of states that can best account for the observed layer of sequence of events. It has long been used in the field of speech recognition where the recorded audio signal is the observed sequence of events and a string of words would form the hidden layer. In power system signal processing a

variation of Viterbi algorithm is applied in [20], [21], [22] where the observed load profile over a prolonged period is the observed layer. Probability distribution is derived from data stored for up to ten days. The hidden layer is then the sequence of known states that can most closely match the observed layer. This algorithm can become very complicated when a large number of states are involved. For N states there are 2^N combinations. The algorithm in [21] performs some optimization to greatly reduce the number of probable combinations. In terms of fault recognition this approach is not ideal because it is difficult to categorize the fault itself as a stage since the nature of fault is unpredictable. Also ideally, fault detection should occur as soon as it happens, but the method in [21] records data over an extended period of time involving several events. Inaction over long periods of time can potentially lead to catastrophic damage, especially at MVDC levels.

A very similar approach is also used by [52] and [60] with good success. Instead of recording data over several load cycles, [52] uses the instantaneous feature of the observed load and recursively solves for the combination of states to determine which loads contribute to the observed waveform. Another method based on the Viterbi algorithm is the Factorial Hidden Markov Model (FHMM), which is used in several papers [61], [62], [63]. The important development in these papers is that they employ an algorithm called the unsupervised learning technique where the training dataset is not required to have one-to-one correspondence with the class type. Getting a training dataset from each class of load can be difficult or impractical

in some applications. This leads to more complex models compared to supervised learning where the relationship between the sample of training dataset and the corresponding class is known. The method in [64] uses a unique fuzzy logic-based approach which is also unsupervised and performs with 85% accuracy. The cognitive electric power meter performs classification based on Bayes' theorem [65], [66]. This is a probability based approach which is suitable for electric monitoring on a large number of loads over an extended period of time.

Matching each observed feature of one event to an array of stored features for all possible events can broadly be categorized as a pattern recognition approach. The most common and intuitive approach is the minimum distance classifier, specifically Euclidian distance classifier. Suppose all the extracted features for any event observed at time t can be combined into a vector X , and an array of vectors m_i contains the mean value of those features for class ω_i . For a system with M classes of loads, m_i is calculated from a pre-programmed database or historical data used for training. The unknown feature vector X is assigned to class ω_i if Euclidian distance between X and m_i is less than Euclidian distance between X and m_j for all $i=j$ [67].

Another family of commonly-used, simple classifiers are nearest neighbor classifiers. The subtle difference between nearest neighbor and minimum distance classifier is that each feature in the feature vector is analyzed independently. If the

algorithm has n different features i.e. X is a vector of length n , then each feature is processed through a minimum distance classifier to determine the nearest feature among all classes. After all features are analyzed, the algorithm looks at which class has most features closest to the observed feature vector. Because of their simplicity and performance many papers use nearest neighbor approaches in some form for their classifier algorithm [38], [39], [68]. An alteration of the nearest neighbor classification is a machine learning technique known as k -means clustering. The variation on nearest neighbor algorithms is that each feature vector is compared to a k moving averages corresponding to the number of loads to be classified and the i th average is shifted once the load is added to load group i within k [69]. The advantage of this approach would allow the averages to shift over time, which may be important to consider for classifying mechanically aging loads.

Neural networks form another family of classifiers that has been considered by a large number of papers [27], [36], [37], [60]. A significant advantage of the neural network architecture branch of machine learning applications is that these architectures can model nonlinearities when multiple layers of nodes are applied in succession during an inference, or classification, operation. And while both traditional artificial and convolutional neural network (ANN/CNN) architectures have been considered for use in both ac and dc distribution system transient analysis in recent years [70], [71], their utility is limited due to the lack of temporal memory. Power distribution systems are causal systems and some loads can exhibit complex

power consumption profiles that can span across multiple sample blocks (for example when monitoring for the cycles of a washing machine). In order to sufficiently employ a ANN/CNN to an ac/dc distribution system, a globally intelligent system must also manage CNN/ANN output snapshots in order to stitch together the responses to provide the temporal awareness.

A recurrent neural network (RNN), and its long short-term memory (LSTM) variant, provide for time-domain signal classification by accounting for previous inputs to influence the classifier output at the current time. Moreover, ANN/CNN layers can also be leveraged simultaneously with an LSTM RNN for feature extraction for better predictor accuracy [72]. RNNs have been applied successively in natural language processing, electrocardiography, and stock market prediction among other fields [73], [74], [75].

2.3.Fault Identification

Using the feature extraction and classifier tools mentioned above several recent research efforts have been made to use microscopic features of load profile to detect faults such as low impedance shunt faults [76], [77], [78], [70], [79] or high impedance series arc faults [80], [81], [82], [83], [84].

Research effort in [76] and [70] is especially pertinent to this research because it targets dc grids in particular. The work in [76] still focuses on the faults on the ac loads attached to the dc grid while [70] discusses faults on several locations on the

grid including both ac and dc sites. The most developed work on shipboard MVDC fault detection using wavelet transforms has been presented in [70] but it still does not cover a comprehensive range of faults, and the algorithm has not been tested on hardware which would test the robustness of the program. Specific contributions of this paper are that it develops a feature vector using the DWT signal energies and it implements an artificial neural network to perform fault detection with a comparison to other fault diagnosis algorithms. Research in [77] provides a comparison of DWT and STFT for feature extraction with a focus on fault diagnosis. Based on various simulated ac faults, [77] concludes that DWT can provide more salient features over the STFT for a majority of faults based on a neural network approach as a classifier.

Considering the series arcing phenomenon, the STFT was used to extract frequency components in [81] paired with an algorithm that can detect the arc based on its frequency composition. The arc detection method is not tested in real time on a processor and the arc current supplied through a parallel capacitor is analyzed instead of the actual current flowing through the air gap. The theory of the algorithm and the modeling work in [81] makes it relevant to this project. Another work of significance is provided in [80] wherein wavelet transforms are used to detect series arcing faults. The work in [80] provides a theoretical algorithm but remains to be applied in real time to a test system. Furthermore, it also needs a network of capacitors which may not be practical for every kind of load but is useful for dc transmission lines.

Residual analysis is another way to perform fault detection by trying to compare measured system parameters against their model estimate values. In [85] and [86], a Kalman filter approach was used to track line current values on individual loads. Large measurement deviations from the filter output signified fault events. Issues posed for using Kalman filter load models is that they require known state-space system models and require linearization which may be a significant detractor for non-linearly switched loads.

Finally, LSTM networks have been used in a few anomaly detection applications in other research fields. Usually these networks require a labeled dataset to train the model to look for anomalous conditions [87], [88], [89]. LSTM autoencoders, which do not require a labeled set, have also been used as fault detectors as well [90], [91]. In [92], Park et al. used an LSTM variational autoencoder (VAE) to detect faults in a robotic assisted feeding application. Unfortunately, while VAE networks offer a robust model tolerant to a wide range of system behaviors, they are not easily trained to perform classification in addition to fault detection. Some machine learning algorithm has been proposed such as STFT cluster analysis [93] and multi-class logistic regression algorithm [94] but the real-time implementation is not mentioned.

3.STFT-LSTM AUTOENCODER BASED DEEP LEARNING APPROACH

3.1.Fourier Transform Data Driven Deep Learning Approach

The proposed approach will be introduced in this section including its key component – autoencoder (AE) with long short-term memory (LSTM) layers network training, Fourier transform feature extraction, and proposed load monitoring algorithm. The proposed approach in this chapter has been published in [95], [96], [97].

3.1.1. Autoencoder with Long Short-Term Memory Layers

As a category of deep learning neural network, the AE has a dumbbell structure as shown in Figure 4. The feature extraction input can be stored in the encoder, then recovered in the decoder part afterwards for the aim of fault identification.

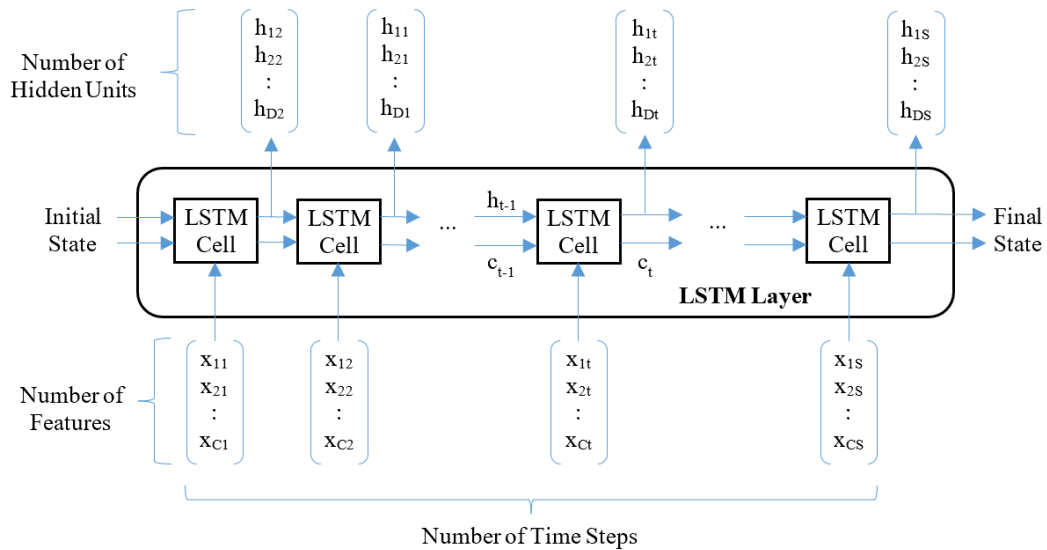


Figure 2. LSTM layer architecture.

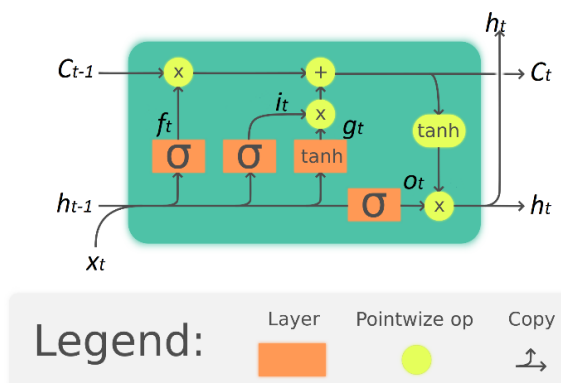


Figure 3. LSTM cell node.

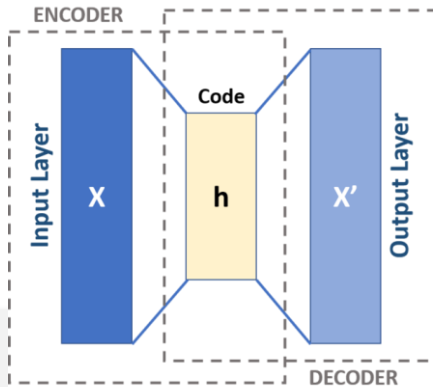


Figure 4. Autoencoder.

In this proposed solution, the AE architecture is used to perform fault identification. To identify a fault, an AE is trained on normal datasets. Any faulty signal input the AE has never experienced is supposed to generate a significant error in reconstruction. An unpredictable and undeterminable reconstruction can be generated because of an unexperienced input signal. The fault is identified by this error between reconstructed and initial signals.

The current waveform monitoring is a type of time series analysis that the LSTM is a suitable candidate. An autoencoder with long short-term memory layers is therefore applied in this time series analysis. Figure 2 represents an overall operation flow of an LSTM layer consisting of LSTM cells. The features in the first time step input the LSTM cell together with random set of initial states i.e. cell state c and hidden units h . Then in each step, a new updated cell state and input features will be fed into the cell to generate the hidden units and next cell state. The hidden units are the cell output and the cell state c contains the previous knowledge learned in each

cell. For the refreshment of the cell state (c), the input gate (i), forget gate (f), gating gate (g) and output gate (o) are being employed in the LSTM cell shown in Figure 3.

Figure 3 explains how the LSTM cell operate in each sampling frequency. The functions in each gate including update, forget and generate cell state and hidden units are illustrated. The trained weights are the input weights $W = [W_f, W_i, W_g, W_o]$, the recurrent weights $R = [R_f, R_i, R_g, R_o]$, and the bias $b = [b_f, b_i, b_g, b_o]$. The i, f, g and o denote the input gate, forget gate, gating gate, and output gate, respectively. The input weights, recurrent weights and biases are obtained through network training.

The cell state updated in each sampling frequency is computed by $C_t = f_t \odot C_{t-1} + i_t \odot g_t$. The hidden units in each sampling step is calculated by $h_t = o_t \odot o_c(C_t)$. At each time step, the input gate is described as $i_t = \sigma_g(W_i \cdot x_t + R_i \cdot h_{t-1} + b_i)$, the forget gate is described as $f_t = \sigma_g(W_f \cdot x_t + R_f \cdot h_{t-1} + b_f)$, the gating gate is $g_t = \sigma_c(W_g \cdot x_t + R_g \cdot h_{t-1} + b_g)$, and the output gate is $o_t = \sigma_g(W_o \cdot x_t + R_o \cdot h_{t-1} + b_o)$. In these calculations, σ_g denotes the gate activation function that is the sigmoid function given by $\sigma(x) = (1 + e^{-x})^{-1}$ to compute the gate activation function.

3.1.2. Network Training

Deep learning is performed on neural networks through training sessions. The aim

of training is to set up the weights and biases in the neural network. There are two forms of training mechanisms for neural networks: supervised and unsupervised learning. In supervised learning, classification labels are supplied with the data and the network weights are adjusted to achieve the best classification performance against the labels. For unsupervised learning tasks, the network is trying to organize around a governing structure to data that is unlabeled. Supervised learning is performed in LSTM by putting a sequence or image to the network and have the network reproduce the input sequence/image. AEs use this unsupervised learning process to adjust their network weights.

The goal of training is to minimize the accuracy loss. An exhaustive search is usually unreasonable to determine the minimum loss because the search space grows exponentially with the number of layers in neural networks. In practice, the gradient descent approach is well-suited for online, or in-service, application because the weights can be adjusted after analysis on only small batches of data. This could be beneficial as to compensate for monitored component aging or other time shifting parameters.

3.1.3. Fourier Transform Feature Extraction

A direct input of time series waveform without feature extraction has only one feature at each time step which is the magnitude of the waveform. It is not enough for accurate waveform classification in the condition that has more than two classes. The short-time Fourier transform (STFT) is therefore chosen so that a number of

STFT harmonic components $X_k[n]$ can be extracted as the feature vectors at each step time. A Fourier transform based feature extraction has been applied in non-intrusive load monitoring applications such as short-time Fourier transform (STFT) cluster analysis based load monitoring. The magnitude of multiple STFT harmonics as feature vector were captured and stored in the database to analyze the feature of normal case, and then compare them with the feature of faulty case to identify faults. The recursive form of STFT - recursive discrete Fourier transform (DFT) is preferred for fast computation in real-time applications shown in Figure 6. In each sampling time step $1/F_s$, an array of length N can be calculated. The magnitude in each element in this array is important for current feature analysis.

The STFT output $X_k[n]$ of the input signal, named harmonic components, is the relevant time-frequency information on waveforms which are fed into the LSTM

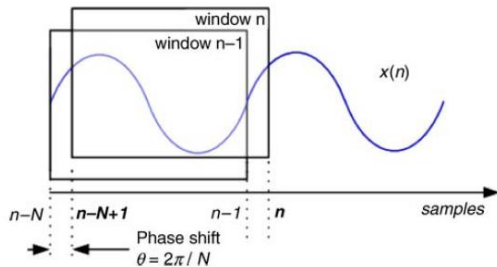


Figure 5. Two consecutive windows.

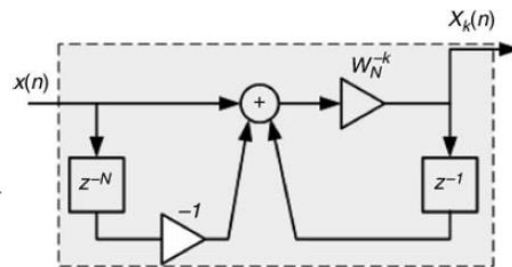


Figure 6. Block diagram for recursive DFT.

RNN AE to reconstruct the input signal. The STFT harmonics $X_k[n]$ in normal operation are different compared to fault cases. Ten STFT harmonic components were shown enough to sufficiently perform the reconstruction. An 10 by L array of harmonic components of the input signal is generated by recursive DFT, where L is

the length of the sample. The ten STFT features are fed into the network in each time step, corresponding to ten components of STFT harmonics.

3.1.4. Load Monitoring Algorithm

The load monitoring algorithm is based on deep learning neural networks. The proposed system includes feature extraction, classification and AE based fault identification as shown in Figure 7. In the feature extraction step, the system implements the input signal measurement and uses STFT to process the measured current to obtain the Fourier transform feature fed into the deep learning neural network. In the next step of classification, the encoder classifies the current waveform as the output of load monitoring. In the fault identification step, the AE recovers the signal and compared it with the real time input signal for error residual calculation. The fault identification system calculates the residuals between original and recovered signal to identify faults.

LSTM encoder-decoder layers includes 30 hidden nodes, sized within the

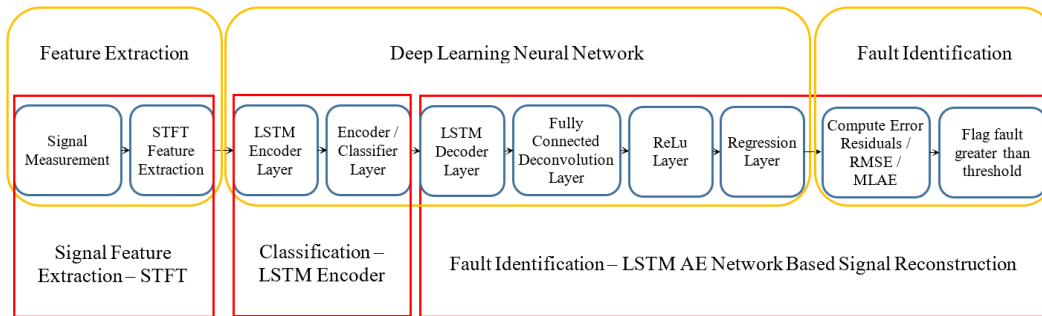


Figure 7. Deep learning based load monitoring.

microcontroller memory constraints. The network is trained in two steps. In the first

step, classified training datasets with the pulsed signal features including its start, ramp, and end stages are being used for training the LSTM encoder layer and classifier layer. This LSTM encoder and classifier layer can output the classification of the signal for the load monitoring purpose. The node size of this LSTM encoder node matches up with the classification number of the load waveform. The input signal is recovered by the AE based signal reconstruction system. Specifically, an 15-node fully connected layer and ReLu layer are employed after the LSTM decoder to reconstruct original signal.

Figure 8 illustrates the fault identification system including two parts to compute and compare the residuals between its original and recovered signal. The two parts are root mean square error (RMSE) and maximum localized absolute error (MLAE). The MLAE is supplemented for small duration disturbances which is hard to detect for RMSE. Whether the MLAE or RMSE are over their individual thresholds (η_1 , η_2) is the criterion of fault identification. An OR logic is used after MLAE and RMSE to identify faults.

The fault identification system calculates and compares the RMSE and MLAE to their respective maximum thresholds reviewed by the receiver operating characteristic (ROC) analysis from the error residuals of the verification datasets. The thresholds are continuously changed at this ROC comprehensive review to trade-off false positive rate (FPR) and false negative rate (FNR).

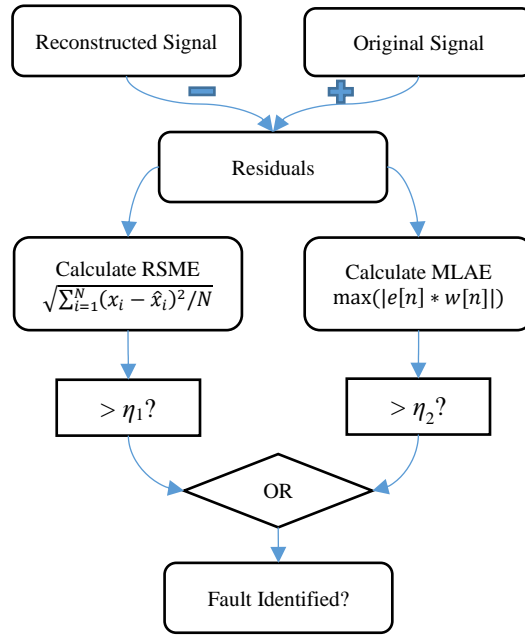


Figure 8. Fault identification system.

3.2. Electric Ship System and Potential Fault Description

A circuit schematic diagram to represent the experimental setup for an electric ship is shown in Figure 9. Three fault monitor subsystems are used to evaluate individual load performance. An overarching load monitor is used to aggregate the outputs of the individual monitor subsystems. The hardware parameters are listed in Table I. Three different types of electric ship loads are linked to the MVDC busbar.

It is difficult to fully enumerate all types of fault conditions that may be present in an electric ship power system. Failure modes for a system will vary with the components used within the system. Therefore

Load 1 (Coil gun)		
$V_{dc}=375V$	$L_{in1}=100\mu H$	$C_{in1}=970\mu F$
$L=2mH$	$V_{out}=300V_{dc\ max}$	$C_{out}=7mF$
$Coil=80\mu H$	$Z_{fault}=15\Omega$	$Load=4mH$
Load 2 (Fixed impedance)		
$L_{in2}=100\mu H$	$N_1:N_2=70:24$	$L_{N1}=51\mu H$
$L_{N2}=6\mu H$	$C_z=100\mu F$	$R_z=100\Omega$
$R_{load}=470\Omega$	$L_{load}=1mH$	$R_{step}=470\Omega$
Load 3 (Propulsion motor)		
$L_{in3}=100\mu H$	$C_{in3}=1.7mF$	PMSM = TI HVPMSMTR

four types of fault have been represented within these hardware loads.

3.2.1. Pulsed Power Load

A coil gun is assembled to emulate advanced pulse-power weapons such as a naval rail gun on an all-electric ship. Its parameters and potential fault locations are illustrated in the Table I and Figure 9 – Load 1. The full-bridge charger is controlled by a DSP chip to maintain each firing cycle of 100ms periodically.

Shunt Fault: Shunt faults are the presence of a short-circuit path between two conductive elements or a conductive element to ground. In the most severe manifestation, the voltage potential between the conductive elements is the limiting factor of the maximum current and power dissipation of the fault. An MVDC shunt fault from the bus voltage to ground potential would consume an enormous amount of energy that could destabilize the distribution if not contained quickly.

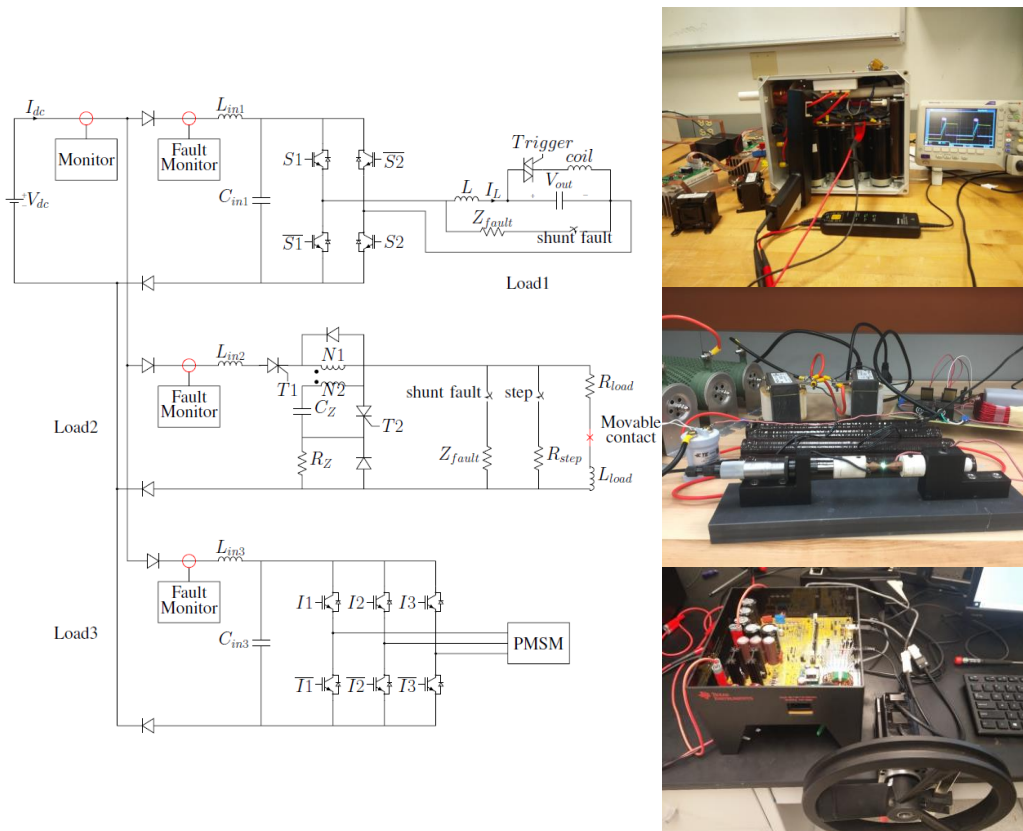


Figure 9. Circuit schematic of dc busbar with electric-ship load hardware prototypes.

Shunt faults are also the most catastrophic form of fault and closest to pulsed load demands. The shunt fault can create a significant pulsating current waveform, so this kind of fault identification is difficult to differentiate from normal pulse currents. In pulsed power loads, Load 1 in Figure 9, the ‘shunt fault’ switch can close for several milliseconds to create shunt faults randomly on purpose.

IGBT Gate Fault: The behavior of IGBT gate fault is similar to open circuit fault. Improper system operation from a variety of sources, this type of fault is a collection of scenarios within a MVDC system leading to improper operation of control

switching. Switching devices can fail in both open and circuit conditions as well as experience parameter drift over time. Improper gate driver timing, software bugs, or malware could also produce erroneous behavior within MVDC distributions. These faults can manifest in a multitude of different ways, making them hard to succinctly characterize; thus all control-failure type faults are lumped into this broad category. In this case, the IGBT gate fault is produced by fluctuating the gate drive signal provided to S1 during the times it should be closed.

3.2.2. Fixed Impedance Load

Fixed impedance load is implemented to emulate the ship service loads. A typical current behaviour in this load is to switch on or off in each one second periodically. The hardware parameters and prototype are illustrated in Table I and Figure 9 - Load 2.

Series Arcing Fault: As a category of high impedance fault, arcing faults are less severe initially but are harder to detect and can lead to significant system damage over time. Dc arcing is more difficult to contain than ac arcing because ac breakers can rely on the zero crossing behavior of the current signal to extinguish the arc. In contrast to shunt faults, series faults introduce a high impedance breakdown of the conductor material reducing the overall load current. The time varying impedance nature of the fault is difficult to model. While identifying series arcing behavior may provide a benefit when considering stochastic load profiles due to the high degree of randomness in both.

In this research, there are two sources of fault within the fixed impedance load. The first source is a shunt fault which is protected by the coupled dc Z-source circuit breaker. The second type of fault, series arcing is not protected by the dc breaker because this type of fault does not exhibit large current swings. The spark generator, movable contact, creates a series arcing fault condition shown in Load 2 of Figure 9.

3.2.3. Propulsion Motor Drive Load

A scale-down permanent magnet machine (PMM) controlled by a three phase inverter was used to emulate the slow transient behavior of electric propulsion system. Fig. 9 – Load 3 shows the hardware setup of this motor drive load.

Partial Blocked Rotor Fault: The behavior of blocked rotor fault is similar to a short circuit fault. Because the PMM is being used here which means that a high current would be very easy to damage the rotor magnet. So only a friction stalling was applied to the inertial flywheel to produce faulty signatures during PMM operation. The flywheel load was manually disturbed at various times during the motor acceleration, deceleration and steady revolutions resulting in abnormal current demands.

3.3. Verification

The classification accuracy can be improved by the Fourier transform feature extraction that is demonstrated in the following current waveform classification test.

3.3.1. Current Waveform Classification

Pulsed Power Load: The trained LSTM networks with or without feature extraction are both implemented to compare the performance improvement. 100 datasets are captured including 60 training datasets and 40 validation datasets. Figure 10 (a) shows the four different stages of pulsed power load operation including pulse start, ramp, end, and n/a. Compared to the ground truth, an accuracy of 98.75% can be achieved under feature extracted classification, compared with 70.12% without feature extraction. All waveforms are identified as n/a because it is the majority of this load classification.

Propulsion Motor Drive Load: The motor drive load is sampled at 100Hz for slow transient capture. Figure 10 (b) shows the four different stages of motor drive load operation including motor steady, accelerating, decelerating, and stalled. Compared to the ground truth, an accuracy of 98.53% can be achieved under feature

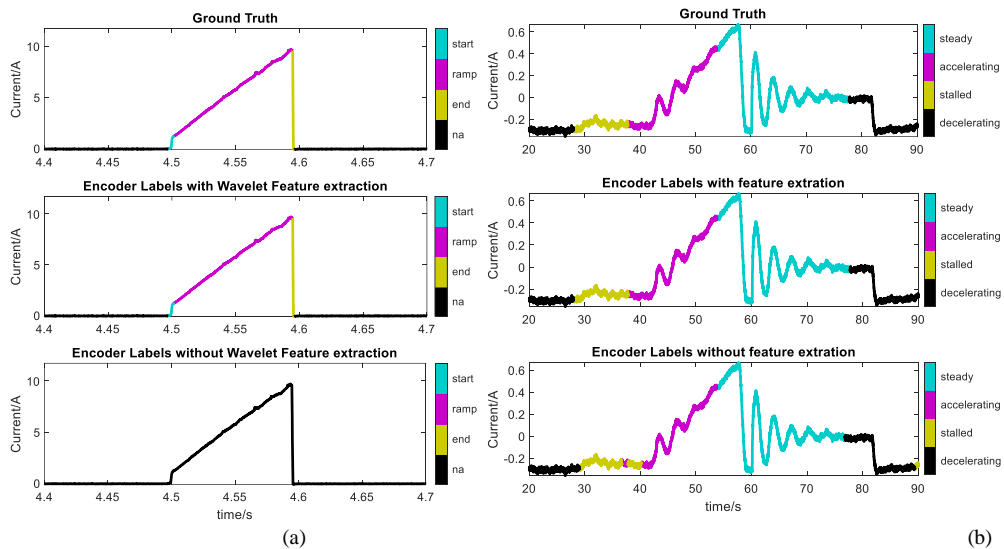


Figure 10. LSTM RNN classification performance of coil gun (a) and propulsion motor drive (b).

extracted classification, compared with 93.75% without feature extraction. The performance is much better than the pulsed power load without feature extraction because the stage classification of motor drive load is more even distribution and there is no short period of stages existed such as ‘start’ and ‘end’ in the pulsed power load.

3.3.2. Fault Identification

The STFT feature in faulty condition is different from normal condition. The autoencoder (AE) can only reconstruct signals similar to normal conditions because AE is only trained from the features in normal condition. It will reconstruct abnormal signals with undetermined waveform when fault happens because AE never experiences the faulty feature in the training process.

Shunt Fault: The validation set of the coil gun includes 30 samples of three-count normal operation pulse trains, 20 samples of a pulse train containing a shunt fault, and 20 samples of a pulse train containing a gate fault. The thresholds of RMSE is 0.09 and MLAE is 0.03 for zero FPR. Fig. 11(a) shows the fault identification of shunt fault case including original and reconstructed signals and residuals calculated from them. In faulty condition in Figure 11(a), the residual has a positive surge at 3.64s corresponding to the largest error residuals.

Because the reconstructed signal is totally different from the original signal. By contrast in normal cases, the residual has no large surges because the reconstructed signal is similar to the original signal. This obvious surge as a sign of anomaly is

used for differentiating this fault from normal condition.

IGBT Gate Fault: The IGBT gate fault identification set-points for the RMSE and MLAE are same as shunt fault and its verification datasets. An

TABLE II IDENTIFICATION CONFUSION MATRIX

Load 1 (Coil gun), RMSE=0.09, MLAE=0.03				
		Network Classification		
		Normal	Fault	
Actual Classification	Normal	30	0	100%
	Fault	1	39	97.5%
		96.8%	100%	
Load 2 (Fixed impedance), RMSE=0.01, MLAE=0.3				
		Network Classification		
		Normal	Fault	
Actual Classification	Normal	10	0	100%
	Fault	0	20	100%
		100%	100%	
Load 3 (Propulsion motor), RMSE=0.13, MLAE=0.06				
		Network Classification		
		Normal	Fault	
Actual Classification	Normal	100	0	100%
	Fault	5	55	91.7%
		95.2%	100%	

exemplar IGBT gate fault behavior and its signal reconstruction are shown in Figure 11(b). The fault event occurs at approximately 4.8s corresponding to the largest error residuals.

Table II shows the composite detector performance against the test dataset of both fault categories. In both cases, an ROC comprehensive review of varying RMSE and MLAE demonstrated the MLAE was more efficient in the short duration gate and shunt fault identification. One fault went undiagnosed, but a review of the undetected gate fault signal showed little to no current disturbance in the original sample because the event occurred during initial pulse ramping when the initial current ramp rate is low.

Series Arc Fault: The validation set of the fixed impedance load includes 10

samples of on-off normal switching operation and 20 samples containing arcing faults. Fig. 11(b) shows the fault identification of arcing fault case including original and reconstructed signals and residuals calculated from them. Table II shows the composite detector performance against the test dataset. The RMSE is 0.01 and

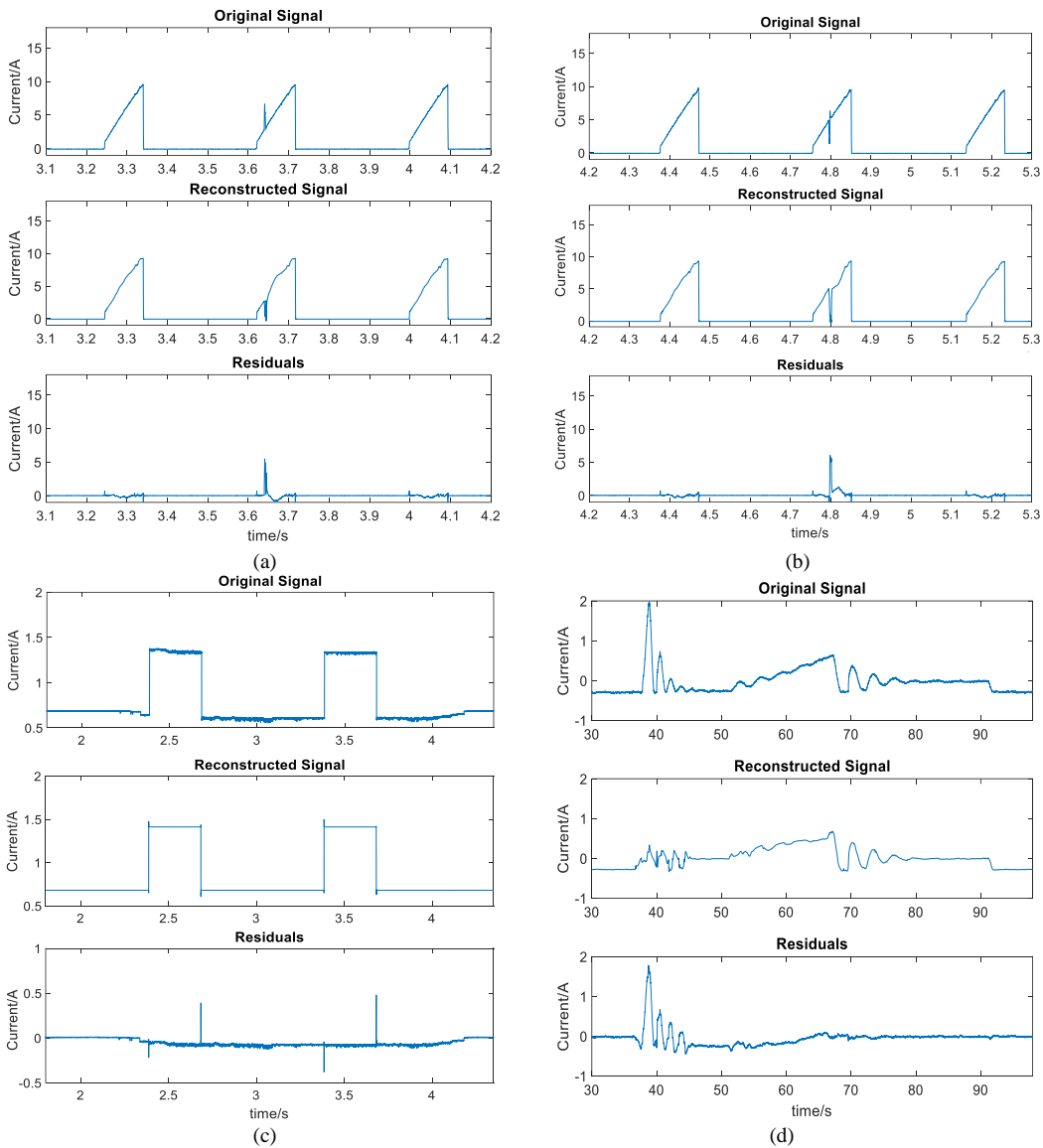


Figure 11. Original and reconstructed signals of shunt fault (a), IGBT gate fault (b), arcing fault (c) and partial blocked rotor fault (d).

MLAE is 0.30 for zero FPR. This detector scheme flagged all series arcing events. An ROC review showed that RMSE was more efficient in the arcing fault detection.

Partial Blocked Rotor Fault: Friction stalling was applied to the inertial flywheel to produce faulty signatures during PMSM operation. The flywheel load was manually disturbed at various times during the motor acceleration, deceleration and steady revolutions resulting in abnormal current demands.

The testing set for the PMSM consisted of 100 acceleration-deceleration cycles, and 60 samples during friction stalling the motor. Fig. 11(d) shows a partial blocked rotor fault. The stalling event causes the motor controller to demand more torque to achieve the commanded speed resulting in current peaking in the load signature. In faulty condition in Figure 11(d), the residual has a positive surge around 40s because the reconstructed signal is totally different from the original signal, which would not happen in normal cases in figure 10(b). This obvious surge as a sign of anomaly is used for differentiating this fault from normal condition.

Table II shows the composite detector performance against the test dataset. The RMSE is 0.13 and MLAE is 0.06. In this case, both RMSE and averaging window error equally helped detect current disturbances. This detector scheme failed to flag several current disturbance events, however the overall fault identification accuracy was relatively high at 91.7%. Increasing the LSTM AE hidden node size to 100 units raised the fault identification accuracy to 95% on the same testing dataset.

3.4. Conclusions

Pulsed power loads are being increasingly deployed on Naval all-electric ships. The deep learning neural network can be used as a tool for load monitoring purpose in these systems. In this article, a Fourier fed long short-term memory autoencoder method was shown to achieve a rapid and accurate result on load monitoring and fault identification of three typical loads operating under four fault cases. Namely, the method was verified using a pulsed power load with a shunt fault and an IGBT gate fault, a fixed impedance load with a series arcing fault, and a motor drive load with a partial blocked rotor fault. In all cases, the method was shown to be highly accurate in identifying faults.

4. WAVELET TRANSFORM DATA-DRIVEN CLUSTERING BASED MACHINE

LEARNING APPROACH

All-electric warships require high power-dense distribution system to power advanced weapon loads. Medium voltage dc (MVDC) power distribution is well suited to fulfill this requirement if certain risks are addressed. A particularly emerging problem is that the advanced pulsating loads draw large currents in extremely short periods of time and behave similarly to the shunt fault. The nature of the load and the operating cycle determines the unique structure of the pulse in time and frequency domains. If the load operating cycle consists of a finite number of transitions, then the corresponding frequency content of the current profile can be used to identify these transients. The wavelet transform is used to extract this useful frequency domain information from the sampled current data. A proposed computationally light data-driven machine learning based fault detection and load monitoring solution extracts the frequency domain features of the observed transient and compares that to a database of stored features to identify the observed transient, then to further identify faults that may create an abnormal disturbance in the load current profile such as arcing and shunt faults. It can be further applied to any load profile with prerequisite of a finite number of repetitive transients during normal condition. This paper focuses on the fault detection only and not for fault isolation while it is simple to achieve isolation capability once the fault was

diagnosed. In final real-time implementation, the recursive Haar stationary wavelet transform (SWT) fed computationally light machine learning is employed to validate the proposed scheme in a single-core Texas Instrument (TI) Digital Signal Processor (DSP) TMS320F28335.

The typical machine learning approach is usually implemented in complicated algorithm with multiple layers and complex structure, which is difficult to do the real-time implementation, especially in a resource-constrained microcontroller. Computationally-light machine learning approach is proposed here for its real time application so the complexity of the algorithm is supposed to be simplified for implementing in microcontrollers. In this paper, a real-time computationally light machine learning algorithm with wavelet transform feature extraction is proposed and validated for fault detection in pulsating power load monitoring of the Naval all-electric ship with MVDC grids. The major contribution of this work concerns the real-time implementation of a simplified k-NN computationally-light machine learning method for dc pulsating load fault detection. This paper focuses on the fault detection only and not for fault isolation while it is simple to achieve isolation capability once the fault was diagnosed. The work of this chapter has been published in [98], [99], [100], [101].

4.1. Machine Learning Based Fault Detection and Load Monitoring

The adopted fault detection and load monitoring solution consists of two distinct parts shown in figure 4. First is databased training, which includes calculation of

unique attributes of an event from raw data in feature extraction, specifically by using Haar wavelet transform to achieve its time-frequency information, then using the information to train the normal database for the preparation of the following classification and detection. The second stage can be referred to as classification monitoring and fault detection stage wherein the real-time observed event is assigned a label based on how its feature compare to those present in the trained database. Specifically, to find the observed event label with most matches, or identify fault if it is different from the majority in the normal database. This section briefly introduces each step of the fault detection and load monitoring algorithm, including feature extraction, event detection, database training, classification monitoring, and fault detection.

4.1.1. Feature Extraction

Time-frequency features are extracted from the discrete-time input current waveform. The common technique of feature extraction is the short-time Fourier transforms (STFT). However, the application of STFT imposes certain limitations on the analysis of the input waveform. The window size of data considered, number of discrete points in the data, and sampling frequency are all fixed which means that the frequency resolution and the range of frequencies analyzed are fixed too. This may limit the ability to detect features from a wide variety of loads. A more advanced harmonic analysis technique called wavelet transform is employed in more recent research that allows the program to zoom into the sampled window of

data and retrieve information at various frequency resolutions.

The wavelet transform was demonstrated to have an advantage over the STFT when trying to extract frequency information from a transient. The wavelet transform is usually implemented using the discrete time wavelet transform (DWT). Figure 12 shows the DWT process for three levels of decomposition [102]. In this approach the input data set is passed through a series of high-pass and low-pass filters in a multi-resolution analysis (MRA) approach to extract coefficients corresponding to the energy in various bands of frequencies at various resolutions.

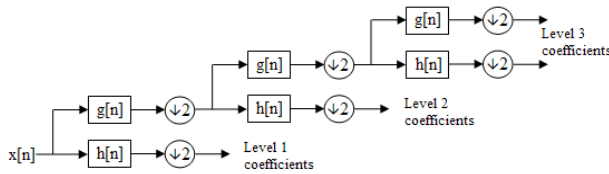


Fig. 12. Three-stage DWT implementation [102].

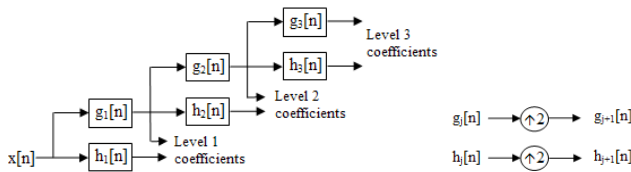


Fig. 13. Three-stage SWT implementation [103].

After passing through the filter stages the input to the next stage is dyadically (2^N) reduced to ensure the output is the same size as the original signal. Many works recently have used DWT instead of STFT to extract time-frequency features from the input data due to

easy access to high-speed multicore processors.

The stationary wavelet transform (SWT) is a variant to the DWT where the filter

TABLE III. EXISTING METHODS COMPERISION.

	STFT	DWT	SWT
Shift invariance	Yes	No	Yes
Dynamically-sized window	No	Yes	Yes
Basis	Sinewaves	Wavelets	Wavelets

stages are dyadically up-sampled rather than down-sampling the signal approximations as in the DWT. In the DWT case, a transient response in the beginning of sample window could have a different response than one occurring at the middle or end of the window. Figure 13 depicts the SWT implementation over three stages [103]. The key benefit to the SWT approach allows the transient signal response to be the same wherever the transient occurs in the sample window. The SWT can also be implemented in real-time but requires more system memory to store each of the filter responses at the same size of the original input signal.

The pros and cons of STFT, DWT and SWT are concluded in Table III. The wavelet transform innately provides a zooming feature with a dynamically-sized window for various transients without operator selection. For other typical feature

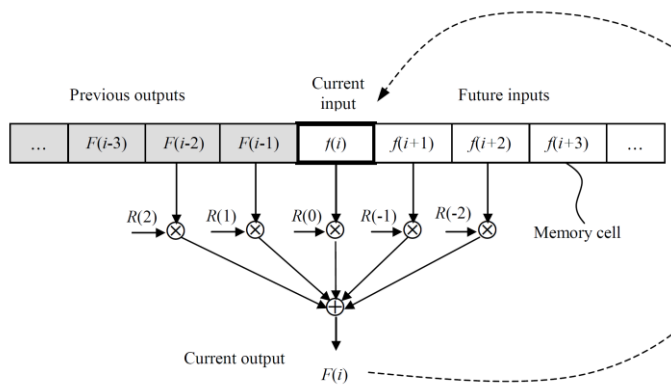


Fig. 14. The recursive 5/3 filters for forward wavelet transform [104].

extraction method such as STFT, a disadvantage is that the analysis window size must be selected using the transient ramp rates for each new transient in the pulse. Its fixed

analysis window requires a signal periodicity to fit infinitely-long sine approximations to extract frequency information, limiting the transient analysis performance for various loads. The wavelet transform is validated to have an advantage over STFT that it innately allows the program to zoom into the sampled window of data and retrieve information at various frequency resolutions. The basis selection has great effects on both speed and performance that will be introduced later.

Wang et al. in [104] presented an algorithm for the recursive calculation of wavelet coefficients for video coding and compression shown in Fig. 14. The recursive wavelet filter approach uses previously calculated filter outputs along with “future” inputs to calculate the filter coefficients for the current time step and is illustrated in. Only odd-sized wavelet filters (5/3 and 9/7) were considered by the algorithm; the filter sizes correspond to the number of filter coefficients in the high-pass and low-pass filters respectively. The algorithm leverages the odd size to center the computation window within the middle of the longest filter applied to the signal. The current input must be delayed until the “future” input is available. This information is usually already available at the time of processing in the context of image and video compression, but a temporal sequence will still require a latency of half the longest filter length. Recursive coefficient computation removes the frame (buffer) requirement for wavelet transform calculation at half the latency of the frame-based approach. Additionally, previously calculated wavelet coefficients

beyond the end filters are discarded, which saves on memory space as the high frequency coefficients are processed and discarded at a faster rate than the lower frequency coefficients. All wavelet coefficients are retained throughout the transformation calculation in frame-based wavelet transformations, and thus have higher memory requirements.

A similar process can be used to recover the wavelet coefficients for other types of wavelets, and is not constrained to filters of odd parity. For real-time monitoring, the recursive Haar SWT presented in equation (1) and (2) is implemented where j is the stage of decomposition, i is the time index, and the input signal is $f[i]$. The Haar wavelet was chosen for its reduced filter size and for the elimination of filter coefficient multiplication operations because the Haar wavelet transform is computed from 2-point differences and sums. It also performed adequately as feature extractors for simulation and experimental data analysis of a pulsed load MVDC system during load shifts and faults. The detail coefficients and approximation coefficients in the current sampling step are calculated from the recursive wavelet filter outputs from previous calculation together with current inputs. Approximation coefficients are achieved by summing the current input signal $f[i]$ to its previous approximation coefficients, then subtracting the input signal outside its filter length. At each stage j , the detail coefficients $D_j[i]$ are computed by the difference between approximations from the finer scale $j - 1$. Each filter stage output is linearly phase-delayed by a fixed amount to synchronize

with the filter-stage output of the lowest frequency band (largest stage of decomposition). For example, the finest detail stage 1 containing high frequency details is delayed by 128 time steps if eight stages of decomposition are required.

$$A_j[i] = 2^{-j/2} \cdot (A_j[i - 1] + f[i] - f[i - 2^j]) \quad (1)$$

$$D_j[i] = 2^{-j/2} \cdot (A_{j-1}[i] - A_{j-1}[i - 2^{j-1}]) \quad (2)$$

For every time step $1/F_s$, an array of length j is calculated by equation (2). Each element in the array is its detail coefficient and magnitude used for current profile analysis. The polarity of detail coefficients in the current has been applied to indicate the feature either increase or decrease to achieve the direction directly.

4.1.2. Event Detection

The pre-processing of event detection includes spectrogram analysis of a typical load profile, surge points identification, and pre-defined event threshold. The features calculated in each sampling step $1/F_s$ seconds are stored and categorized only when an event happens. The events are predefined by user selection on the algorithm parameter i.e. event threshold. A time-frequency approach is chosen in which the spectrum in full cycle is observed and its salient points in particular detail coefficient in SWT can be thresholds which are used to identify specific event.

4.1.3. Database Training

Figure 15 illustrates key steps in the load monitoring system including database training and classification monitoring. Database training requires a fault-less

controlled operation of the load during which the events occur in a known sequence. The sequence of events is known prior to operation and programmed in the scheme through an event-sequence-array (ESA). The ESA is an array including the order of labelled event expected to happen in sequence defined by users.

In each sampling frequency of event detection, an array of features calculated from sampling data are stored in memory according to ESA defined by user. Memory allocation is determined by the length of ESA and number of unique event labels. ESA must be provided before training and all normal operations are secured to happen with no faults during the database training. After the collection of ESA database by the end of training, a three-dimensional statistical matrix has been calculated including the mean, maximum and minimum values based on the ESA database saved in memory.

4.1.4. Classification Monitoring

The typical nearest neighbor approach or other more complex algorithms cannot be implemented in one sampling frequency and therefore cannot be implemented in run-time in this specific DSP. A computationally light machine learning approach is proposed to classify the observed feature in real time instead of k-nearest neighbor approach: A 2-D Boolean Match Matrix is populated first. Then the input observed feature can be regarded as TRUE if it is within the minimum and maximum values of that feature in statistical matrix. Event label with most matches is declared the label for observed event. If several events have number of TRUE matches within

25% of each other, the distance calculation is performed. In that case the distance from mean is calculated only for the features with FALSE match for the competing event labels. Event label with least distance is declared the label for observed event. The process of this classification monitoring is illustrated in Fig. 15.

4.1.5. Shunt Fault Detection

Most shunt fault analysis is performed with a low fixed impedance resistance in parallel to operating loads. As the shunt fault is activated in this load, the resultant power demand is a step load change, or ramp if arc inductance is included in modeling. Circuit protection based on these models will naturally rely on detecting the sharp ramp rate on supply current to meet the lower system impedance. These circuit protection methods cannot be relied on to protect naval MVDC systems employing pulsed load technologies which also demand high current ramp rates.

According to the previous classification, a modification is used for shunt fault detection shown in Fig. 15. Using a time domain method such as di/dt , the fault event is almost same as the normal pulsed event, while their frequency spectrum can be distinguished. Classification monitoring will force a label on the faulty event with the closest match of recorded event. However, a threshold can be defined on number of labels to exhibit a TRUE match in order to define a fault. Therefore in matrix matching step of Fig. 15, if the real-time feature cannot match up with any labelled event over the threshold of $j - n$, it is labelled as fault condition, where n is the tolerance parameter. Choice of n is an engineer's decision based on confidence in

database training, natural variation in load profile, and the required sensitivity of the system. A small n may lead to some normal event with slight difference to be labelled as fault condition, a large n may regard a fault as normal labelled event.

4.1.6. Arc Fault Detection

Shunt faults manifest in arcing phenomenon if the short-circuit path is over air, as well as series faults discussed in this subsection. Arcing is the electrostatic breakdown of air which occurs over potential distances at 3 MV/m, making this a particular concern for MVDC distributions. The series arcing fault detection method can take advantage of the detail coefficients at low stages on arcing current. The feature $|D_j[i]|$ under stage 3 can be stored in database training and an array of length j at low stages can be calculated in each sampling step $1/F_s$ seconds. If it is higher than its database training average value, it would be regarded as an arcing fault. The flow diagram of arc fault detection is illustrated in Fig. 15. The core parts of overall algorithm including database training, classification monitoring and fault detection are implemented in Matlab/Simulink, which can be compiled into an out file that loads directly to the TI C2000 DSP by embedded coder support package for Texas Instruments C2000 processors in Simulink.

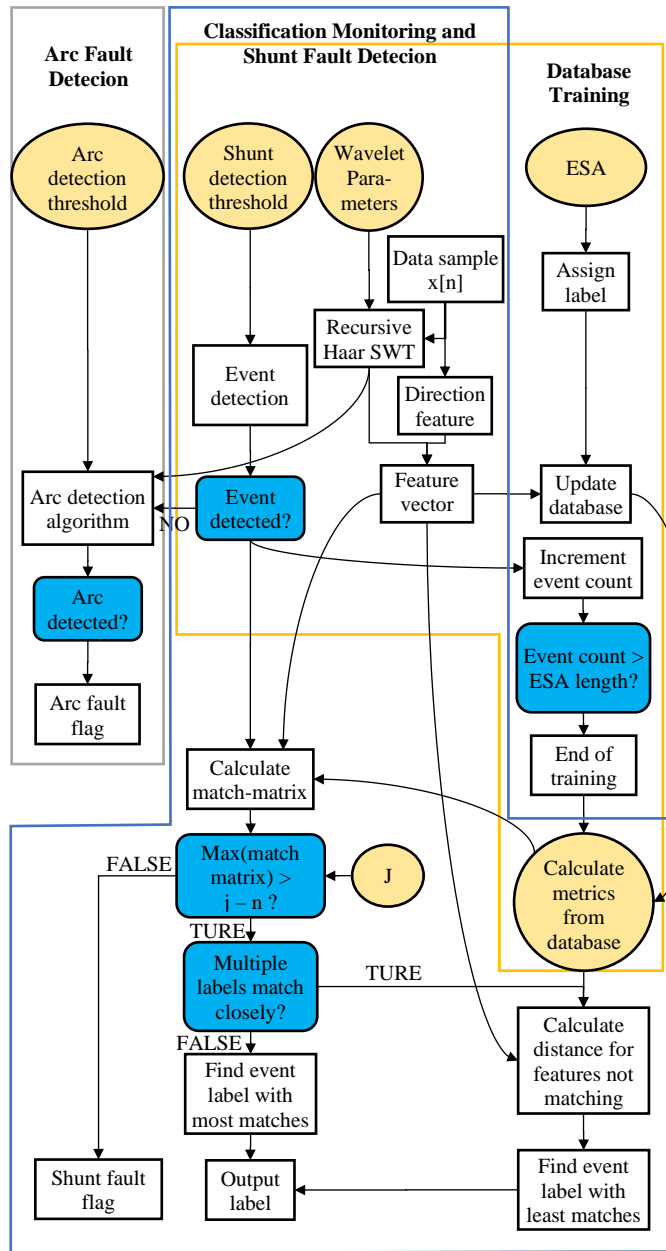


Fig. 15. Flow diagram of data-driven machine learning based fault detection and load monitoring algorithm.

4.2. Simulation Results

The overview of Naval shipboard dc pulsating loads is introduced first. Then the simulation results of the machine learning based fault detection and load monitoring algorithm are described in this section, comparing to real-time experimental result in section VI.

4.2.1. Naval Shipboard Dc Pulsating Loads

This subsection introduces the dc pulsed loads on naval shipboard power system

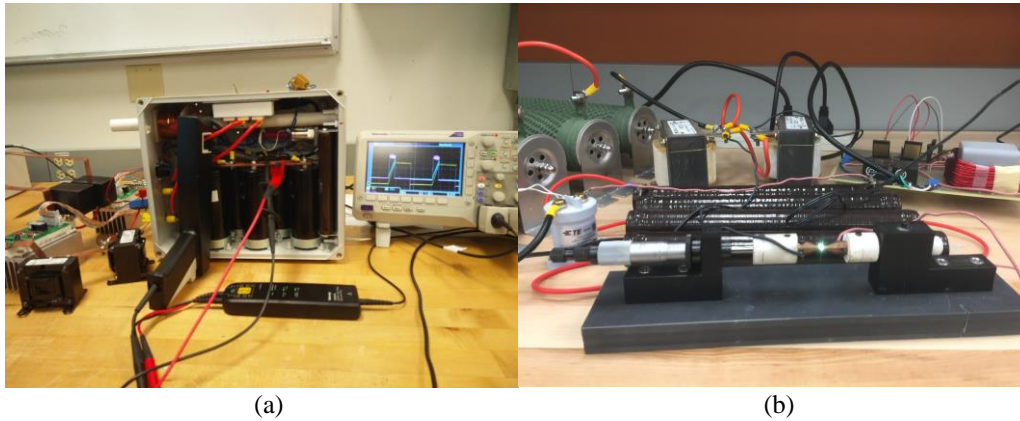


Fig. 16: Naval pulsed-power load hardware prototype. (a) Coil gun pulsed-power load and (b) fixed impedance load.

and their parameters. The scaled-down naval shipboard dc pulsed loads are shown in Fig. 16(a) and 16(b). Two naval dc loads consists of pulsed-power coil gun (Load 1) and fixed impedance (Load 2). Both typical loads represent different dc pulsed loads with fast transient for testing the algorithm performance for different naval dc pulsed loads. Shunt fault, IGBT fault and arcing fault are also generated

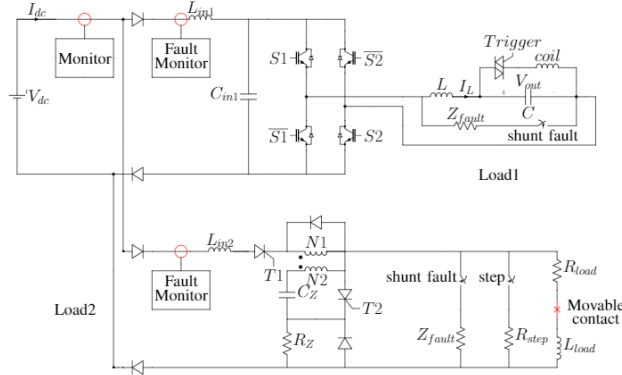


Fig. 17. Circuit schematic of pulse load hardware prototypes.

TABLE IV. HARDWARE DESIGN PARAMETERS.

Load 1 (Coil gun)		
$V_{dc}=375V$	$L_{in1}=100\mu H$	$C_{in1}=970\mu F$
$L=2mH$	$V_{out}=300V_{dc\ max}$	$C_{out}=7mF$
Coil=80 μH	$Z_{fault}=15\Omega$	Load=4mH
Load 2 (Fixed impedance)		
$L_{in2}=100\mu H$	$N_1:N_2=70:24$	$L_{N1}=51\mu H$
$L_{N2}=6\mu H$	$C_z=100\mu F$	$R_z=100\Omega$
$R_{load}=470\Omega$	$L_{load}=1mH$	$R_{step}=470\Omega$

intentionally in these loads to validate the protection algorithm. Design parameters of these naval dc pulsed loads are listed in Table IV. For each type of fault identification, they have their own MCU in each load so that it can be easily identified as specific type of fault.

4.2.2. Coil Gun with Shunt Fault and IGBT Gate Fault

The scaled-down naval shipboard dc pulsed power loads are shown in Fig. 16. A coil gun represent dc pulsed power loads with fast transient for testing the algorithm performance. Shunt fault, and IGBT fault are generated intentionally in this load to validate the protection algorithm. Design parameters of this dc pulsed load are listed

in Table IV. An H-bridge charger has been implemented to charge the coil paralleled capacitor by constant 10A in each cycle. An SCR switch is used to fire the coil gun when the voltage of coil paralleled capacitor reached 300Vdc, and it takes about 200ms in each firing pulse cycle.

The location where the shunt fault is placed across the full-bridge charger is shown in Fig. 17 resulting in a positive spike in the current waveform. The IGBT gate fault is due to improper system operation that could happen from a variety of sources such as improper control signal and gate firing sequences or harmonic distortion events. It is made by control error in the gate driver resulting in a negative surge in the current waveform. Both are challenging to pick based on current threshold.

In each pulse, the start and end are transient components selected as classified event 1 and 2 as shown in Fig. 18 and Fig. 19. During wavelet transform data analysis, $D_j[i]$ profile over one load cycle has two distinct surges. The event detection threshold is selected to be 0.4 according to the wavelet transform data analysis result $D_j[i]$ and the intention to have two labelled events during each normal cycle. There were 150 cycles of the normal load profile used to create a database in training. Each time the detail coefficient is over the event threshold, this event is detected and saved as a wavelet feature vector in the database memory. After

training, certain faults are created. For the label sign of each event, it is defined that event 1 is +1, event 2 is +2, and fault is -1. They raised respectively when happening. The performance of load monitoring is shown in Table V. As can be seen, the method was able to achieve 1% false positives and 3.33% false negatives in the example coil gun scenario. For the shunt fault and IGBT gate fault, the distinguish can be achieved by adding discriminator based on their time and frequency domain information. The discriminator is not used here because both faults are shunt fault (one is positive, the other is negative shunt fault), and the aim of this solution is to detect fault only.

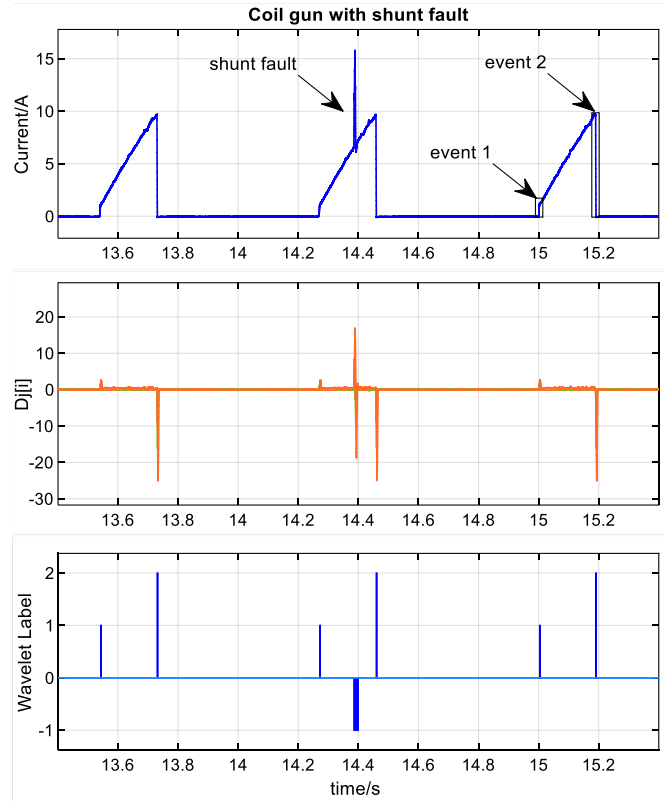


Fig. 18. Simulation result of coil-gun load with shunt fault.

3.33% false negatives in the example coil gun scenario. For the shunt fault and IGBT gate fault, the distinguish can be achieved by adding discriminator based on their time and frequency domain information. The discriminator is not used here because both faults are shunt fault (one is positive, the other is negative shunt fault), and the aim of this solution is to detect fault only.

4.2.3. Fixed Impedance with Series Arcing Fault

Fixed load is built up for emulating the ship service loads such as lighting system, central heating system etc.. It usually operates periodically as a step change in power of the load. Series arcing faults should be detected and isolated quickly because they

can pose a fire hazard and personnel shock hazard. A movable contact shown in Fig. 17 is applied for generating arcing fault, so the series arcing fault algorithm is validated through this setup.

In simulation results, two significant transient parts i.e. start and end are selected as labelled event 1 and event

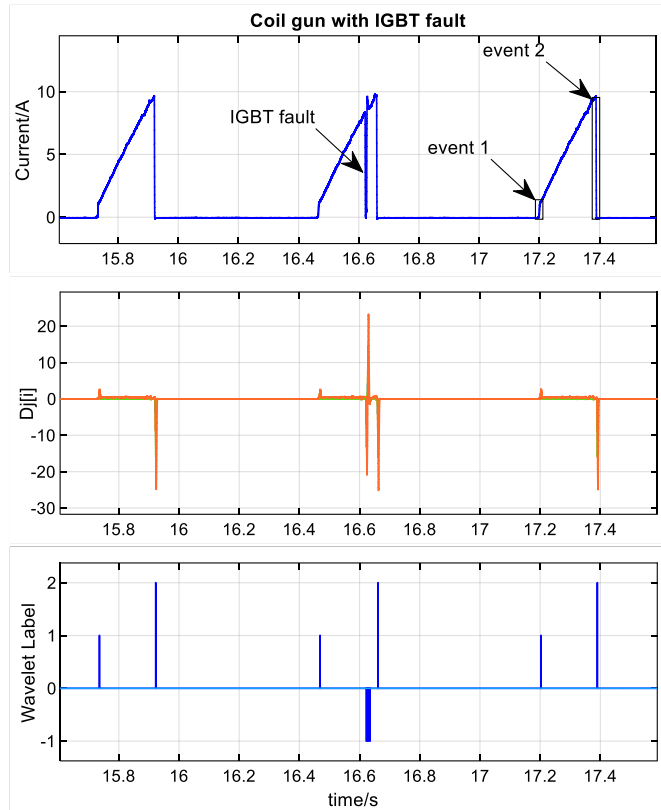


Fig. 19. Simulation result of coil-gun load with IGBT fault.

2 in Fig. 20. The sampling frequency has been kept same as coil gun, and the event threshold is chosen 0.8 according to the detail coefficients of the fixed impedance load. There were 150 cycles of the normal load profile are used to create a database in training. Each time an event is detected a feature vector is saved in memory. After training, certain faults are created. The label sign of event 1 (+1), event 2 (+2), and fault (-1) are raised when their respective case happens. The disturbance created by

the arc generation device is not large enough to trigger a normal event but the arc fault detection is able to identify it and raise -1 flags continually during duration of the arc. The performance and detection parameters are listed in Table V.

4.3. Real-time DSP Implementation

The data-driven machine learning algorithm with

wavelet transform based feature vectors has been implemented in the TI DSP model TMS320F28335. Computation requirements become high with higher sampling frequency and more event labels. The sampling frequency was therefore reduced compared to simulation verification for some cases. Because the processing speed

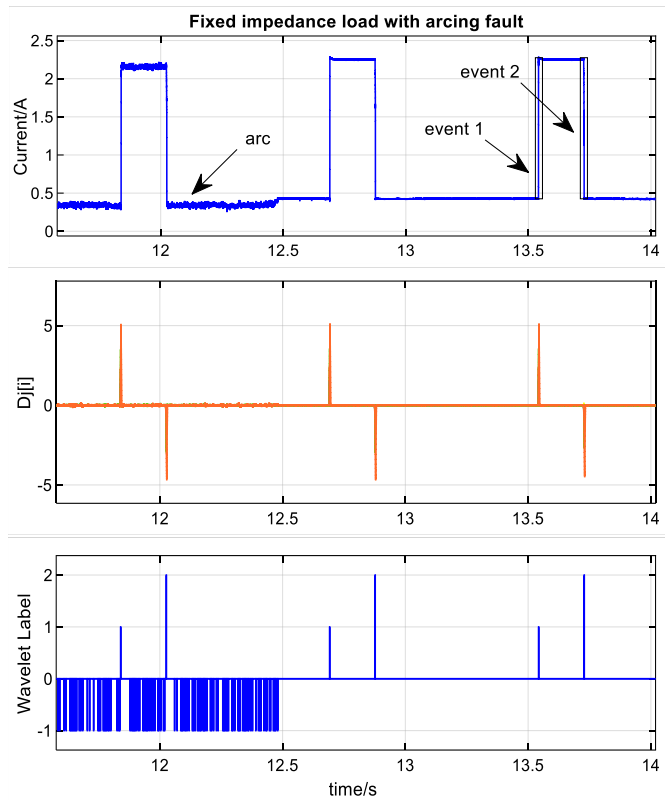


Fig. 20. Simulation result of fixed impedance load with series arcing fault.

TABLE V. Detection Parameters and Performance Summary of Simulation and Experimental Results.

	Coil Gun		Fixed impedance	
	Simulation	DSP	Simulation	DSP
Event threshold	1.2	1.2	0.8	0.8
j	8	8	8	8
Arcing threshold	na	na	0.0015	0.0015
F _s	10 kHz	5 kHz	10 kHz	5 kHz
Detection time	100 μs	200 μs	100 μs	200 μs
Length of ESA	300	20	300	20
Event per cycle	2	2	2	2
n	2	2	2	2
Event 1 appearance	149	12	150	12
% correct labeled	99.3%	100%	100%	100%
Event 2 appearance	148	12	149	12
% correct labeled	98.6%	100%	99.3%	100%
Normal load cycles	150	12	150	12
Fault event cycles	30	4	50	60
False positive	1.00%	0%	0.50%	0%
False negative	3.33%	0%	4.00%	0%

is 150MHz, the single-core DSP cannot finish the computation within 100μs as simulation, the sampling frequency F_s is therefore down to 5kHz so that the computation can complete within 200μs. The fastest reaction is one sampling time, equal to $1/F_s$. In simulation, the detection time is 100μs, by contrast in the real time implementation, it is 200μs because the sampling frequency decreases to 5kHz. Smaller training period or shorter ESA are required due to the memory and practical constraints. The ESA used for real-time implementation are therefore fifteen times shorter than those in database training in offline simulations.

4.4. Experimental Results

The DSP experimental results of real-time fault detection and load monitoring algorithm are described in this section, validating the simulation results in section IV.

4.4.1. Coil Gun with Shunt Fault and IGBT Gate Fault

Ten normal load currents pulses are used in database training which are 15 times shorter than offline simulation. In Fig. 21, the first two pulsed are the end of training process then the rise step of 3rd pulsed is used for database calculation including maximum, minimum and mean value of previous 20 input datasets. Since then, the system starts the classification and fault detection. As shown in Fig. 21, in total four shunt faults are created intentionally including two positive shunt faults and two negative shunt faults, and all are identified correctly. The classification of start and

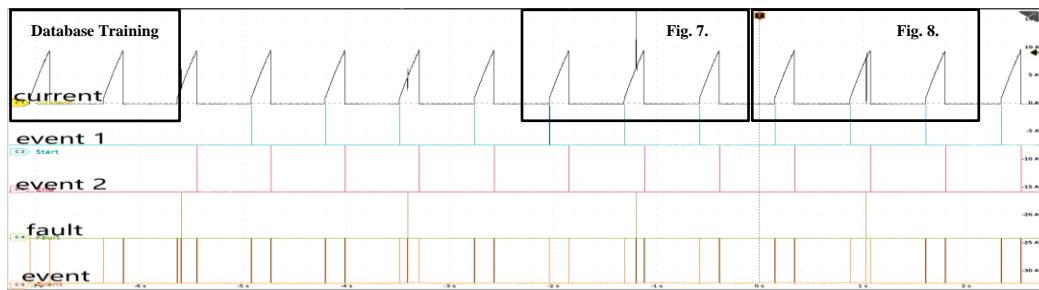


Fig. 21. Real-time experimental result of fourteen load cycles with normal and faulty operations of the coil gun.

end in each pulse are also labelled accurately with no false positives. The zoomed waveforms of either shunt faults or normal operation are same as the simulation Fig. 18 and Fig. 19. The load monitoring parameters and performance are concluded

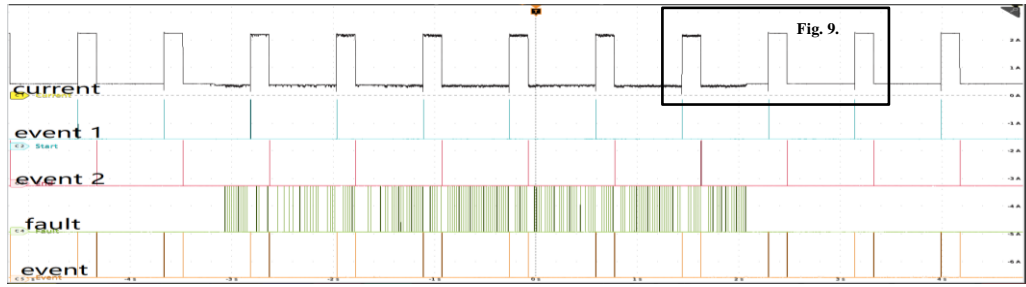


Fig. 22. Real-time experiment result of eleven load cycles with normal and faulty operations of the fixed load.

in Table III, with a fast detection time of 200 μ s, no false positives and no false negative, validating the simulation results in section III. For the shunt fault and IGBT gate fault, the distinguish can be achieved by adding discriminator based on their time and frequency domain information. The discriminator is not used here because both faults are shunt fault (one is positive, the other is negative shunt fault), and the aim of this solution is to detect fault only.

4.4.2. Fixed Impedance with Series Arcing Fault

The detection parameters of fixed impedance load are listed in Table III including the additional arc threshold. Ten normal cycles of load currents are applied to database training in the microprocessor. The response for normal load cycles and series arcing faults are shown in Fig. 22. The series arcing fault detection is zoomed shown in Fig. 20. All the events are detected and identified accurately with no false positives. The algorithm parameters and method performance for this load are shown in Table III, with a fast detection time of 200 μ s, no false positives and no false negatives.

4.5. Conclusions

Pulsed power loads are extensively deployed on naval shipboard medium-voltage dc power systems. The pulse profiles of these loads create challenges to load monitoring systems in future shipboard MVDC grids. A wavelet transform-based computationally light machine learning algorithm for Naval dc pulsating loads are applied in shipboard power system application and can be further applied to any load profile with prerequisite of a finite number of repetitive transients during normal condition.

The real-time implementation of this algorithm achieves a rather quick and high accuracy on fault identification of both typical pulse-power loads with three typical faults i.e. an electromagnetic coil gun load with shunt fault and IGBT gate fault, and a fixed impedance load with series arcing fault. Lower false positives and higher true positives are achieved in both simulation and real-time implementation. Any fault or disturbance that creates an unexpected transient in the load profile will be quickly and reliably diagnosed and a trigger can be sent for protection.

5.CONTRIBUTIONS AND FUTURE WORKS

To summary, two types of AI approaches are proposed including wavelet data-driven clustering-based machine learning approach and STFT-fed LSTM autoencoder-based deep learning approach. Pulsed power loads are being increasingly deployed on naval all-electric ships. The deep learning neural network can be used as a tool for load monitoring purpose in these systems. In this article, a Fourier fed long short-term memory autoencoder method was shown to achieve a rapid and accurate result on load monitoring and fault identification of three typical loads operating under four fault cases. Namely, the method was verified using a pulsed power load with a shunt fault and an IGBT gate fault, a fixed impedance load with a series arcing fault, and a motor drive load with a partial blocked rotor fault. In all cases, the method was shown to be highly accurate in identifying faults. A wavelet transform-fed computationally light machine learning algorithm for Naval dc pulsating loads are applied in shipboard power system application and can be further applied to any load profile with prerequisite of a finite number of repetitive transients during normal condition.

The real-time implementation of this algorithm achieves a rather quick and high accuracy on fault identification of both typical pulse-power loads with three typical faults i.e. an electromagnetic coil gun load with shunt fault and IGBT gate fault, and a fixed impedance load with series arcing fault. Lower false positives and higher true positives are achieved in both simulation and real-time implementation. Any

fault or disturbance that creates an unexpected transient in the load profile will be quickly and reliably diagnosed and a trigger can be sent for protection.

For the future works, the accuracy guarantee from source-side measurement and monitoring by algorithm optimization can be the further research direction. The LSTM autoencoder-based deep learning approach can be real-time implemented in microcontrollers.

BIBLIOGRAPHY

- [1] H. Woud and D. Stapersma, Design of Propulsion and Electric Power Generation Systems, London: IMarEST, 2008.
- [2] Y. Ma, K. Corzine, A. Maqsood, F. Gao and K. Wang, "Stability Assessment of Droop Controlled Parallel Buck Converters in Zonal Ship DC Microgrid," 2019 IEEE Electric Ship Technologies Symposium (ESTS), 2019, pp. 268-272.
- [3] N. Doerry and J. Amy, "Design Considerations for a Reference MVDC Power System," in SNAME Maritime Convention, Bellevue, 2016.
- [4] S. Leeb, K. J.L., W. Wichakool, Z. T. C. Remscrim, J. Goshorn, K. Thomas, R. Cox and R. Chaney, "How Much DC Power is Necessary," Naval Engineers Journal, vol. 122, no. 2, pp. 79-92, 2010.
- [5] S. Patil and A. E.W., "Real-time continuous wavelet transform on a DSP processor," Journal of Medical Engineering and Technology, vol. 33, no. April, pp. 223-231, 2009.
- [6] J. Gillis and W. Morsi, "Non-Intrusive Load Monitoring Using Orthogonal Wavelet Analysis," in IEEE Canadian Conference on Electrical and Computer Engineering, 2016.

- [7] R. Bonfigli, M. Severini, S. Squartini, M. Fagiani and P. F., "Improving the Performance of the AFAMAP Algorithm for Non-Intrusive Load Monitoring," in IEEE Congress on Evolutionary Computation, 2016.
- [8] N. Henao, S. Kelouwani, K. Agbossou and Y. Dub, "IEEE International Symposium on Industrial Electronics," in Active Power Load Modeling Based on Uncertainties for Non Intrusive Load Monitoring, 2016.
- [9] T. DeNucci, R. Cox, S. Leeb, J. Paris, M. T.J., C. Laughman and G. W.C., "Diagnostic Indicators for Shipboard Systems Using Non-Intrusive Load Monitoring," in IEEE Electric Ship Technologies Symposium, 2005.
- [10] R. Cox, P. Bennett, M. T.D., P. J. and L. S.B., "Using the Non Intrusive Load Monitor for Shipboard Supervisory Control," in IEEE Electric Ship Technologies Symposium, 2007.
- [11] P. Lindahl, S. Leeb, J. Donnal and B. G., "Noncontact Sensors and Nonintrusive Load Monitoring (NILM) aboard the USCGC Spencer," in IEEE AUTOTESTCON, 2016.
- [12] P. Lindahl, D. Green, G. Bredariol, A. Abouliah, J. Donnal and S. Leeb, "Shipboard Fault Detection Through Nonintrusive Load Monitoring: A Case Study," IEEE Sensors Journal, vol. 18, no. 21, pp. 8986-8995, 2018.
- [13] M. Zeifman and K. Roth, "Nonintrusive appliance load monitoring: review and outlook," IEEE Trans. Consumer Electronics, vol. 57, no. 1, p. 7684, 2011.

- [14] G. Hart, "Nonintrusive appliance load monitoring," Proceedings of the IEEE, vol. 80, no. 12, pp. 1870-1891, 1992.
- [15] A. Cole and A. Albicki, "Data extraction for effective non-intrusive identification of residential power loads," in IMTC/98 Conference Proceedings. IEEE Instrumentation and Measurement Technology Conference. Where Instrumentation is Going, 1998.
- [16] A. Cole and A. Albicki, "Algorithm for nonintrusive identification of residential appliances," in IEEE International Symposium on Circuits and Systems, 1998.
- [17] R. Zmeureanu and L. Farinaccio, "Using a pattern recognition approach to disaggregate the total electricity consumption in a house into the major end-uses," Energy and Buildings, vol. 30, no. 3, pp. 245-259, 1999.
- [18] M. Marceau and R. Zmeureanu, "Nonintrusive load disaggregation computer program to estimate the energy consumption of major end uses in residential buildings," Energy Conversion and Management, vol. 41, no. 13, pp. 1389-1403, 2000.
- [19] J. Powers, B. Margossian and B. Smith, "Using a rule-based algorithm to disaggregate end-use load profiles from premise-level data," IEEE Computer Applications in Power, vol. 4, no. 2, pp. 42-47, 1991.

- [20] M. Baranski and J. Voss, "Nonintrusive appliance load monitoring based on an optical sensor," in 2003 IEEE Power Tech Conference Proceedings, Bologna, 2003.
- [21] M. Baranski and J. Voss, "Detecting patterns of appliances from total load data using a dynamic programming approach," in IEEE International Conference on Data Mining, 2004.
- [22] M. V. J. Baranski, "Genetic algorithm for pattern detection in NIALM systems," in IEEE International Conference on Systems, Man and Cybernetics, 2004.
- [23] A. Ruzzelli, C. Nicolas, A. Schoofs and G. O'Hare, "Real-Time Recognition and Profiling of Appliances through a Single Electricity Sensor," in IEEE Communications Society Conference on Sensor and Ad Hoc Communications and Networks (SECON), 2010.
- [24] M. Figueiredo, A. Almeida and B. Ribeiro, "An Experimental Study on Electrical Signature Identification of Non-Intrusive Load Monitoring (NILM) Systems," in International Conference on Adaptive and Natural Computing Algorithms, 2011.
- [25] F. Sultanem, "Using appliance signatures for monitoring residential loads at meter panel level," IEEE Transactions on Power Delivery, vol. 6, no. 4, 1991.

- [26] S. Leeb, A Conjoint Pattern Recognition Approach to Nonintrusive Load Monitoring, Cambridge: MIT PhD Thesis, 1993.
- [27] L. Norford and S. Leeb, "Non-intrusive electrical load monitoring in commercial buildings based on steady-state and transient load-detection algorithms," *Energy and Buildings*, vol. 24, no. 1, pp. 51-64, 1996.
- [28] S. Leeb, S. Shaw and J. Kirtley, "Transient event detection in spectral envelope estimates for nonintrusive load monitoring," *IEEE Transactions on Power Delivery*, vol. 10, no. 3, pp. 1200-1210, 1995.
- [29] S. Shaw, S. Leeb, L. Norford and R. Cox, "Nonintrusive Load Monitoring and Diagnostics in Power Systems," *IEEE Transactions on Instrumentation and Measurement*, vol. 57, no. 7, pp. 1445-1454, 2008.
- [30] S. Shaw, C. Abler, R. Lepard, D. Luo, S. Leeb and L. Norford, "Instrumentation for High Performance Nonintrusive Electrical Load Monitoring," *Journal of Solar Energy Engineering*, vol. 120, no. 3, pp. 224-229, 1998.
- [31] U. Khan, S. Leeb and M. Lee, "A multiprocessor for transient event detection," *IEEE Transactions on Power Delivery*, vol. 12, no. 1, pp. 51-60, 1997.
- [32] J. Paris, J. Donnal and S. Leeb, "NilmDB: The non-intrusive load monitor database," *IEEE Transactions on Smart Grid*, vol. 5, no. 5, pp. 2459-2467, 2014.

- [33] K. Lee, S. Leeb, L. Norford, P. Armstrong, J. Holloway and S. Shaw, "Estimation of variable-speed-drive power consumption from harmonic content," *IEEE Transactions on Energy Conversion*, vol. 20, no. 3, pp. 566-574, 2005.
- [34] P. Lindahl, D. Green, G. Bredariol, A. Aboulhian, J. Donnal and S. Leeb, "Shipboard Fault Detection Through Nonintrusive Load Monitoring: A Case Study," *IEEE Sensors Journal*, vol. 18, no. 21, pp. 8986-8995, 2018.
- [35] S. Shaw, *System Identification Techniques and Modeling for Nonintrusive Load Diagnostics*, Cambridge: MIT PhD Thesis, 2000.
- [36] C. Laughman, K. L., R. Cox, S. Shaw, S. Leeb, L. Norford and P. Armstrong, "Power Signature Analysis," *IEEE Power and Energy Magazine*, vol. 1, no. 2, pp. 56-63, 2003.
- [37] D. Srinivasan, W. Ng and A. Liew, "Neural-network-based signature recognition for harmonic source identification," *IEEE Transactions on Power Delivery*, vol. 21, no. 1, pp. 398-405, 2006. [38] M. Berges, G. E., H. Matthews and L. Soibelman, "Learning Systems for Electric Consumption of Buildings," in *International Workshop on Computing in Civil Engineering*, Austin, 2009.
- [39] M. Berges, E. Goldman, H. Matthews and L. Soibelman, "Enhancing Electricity Audits in Residential Buildings with Nonintrusive Load Monitoring," *Journal of Industrial Ecology*, vol. 12, no. 5, pp. 844-858, 2010.

- [40] M. Ribeiro, C. Marques, C. Duque, A. Cerqueira and J. Pereira, "Power quality disturbances detection using HOS," in IEEE Power Engineering Society General Meeting, 2006.
- [41] Y. Su, L. K.L. and C. H.H., "Feature Selection of Non-intrusive Load Monitoring System Using STFT and Wavelet Transform," in IEEE 8th International Conference on e-Business Engineering, Beijing, 2011.
- [42] W. Chan and A. L. L. So, "Harmonics load signature recognition by wavelets transforms," in International Conference on Electric Utility Deregulation and Restructuring and Power Technologies, London, 2000.
- [43] C. Duarte, P. Delmar, K. Goossen, K. Barner and E. Gomez-Luna, "Non-intrusive load monitoring based on switching voltage transients and wavelet transforms," in 37 Future of Instrumentation International Workshop (FIIW) Proceedings, Gatlinburg, 2012.
- [44] H. Chang, "Non-Intrusive Demand Monitoring and Load Identification for Energy Management Systems Based on Transient Feature Analyses," Smart Grid and the Future Electrical Network, vol. 5, no. 11, pp. 4569-4589, 2012.
- [45] H. Chang, K. Chen, Y. Tsai and L. W.J., "A New Measurement Method for Power Signatures of Nonintrusive Demand Monitoring and Load Identification," IEEE Transactions on Industry Applications, vol. 48, no. 2, pp. 764-771, 2011.

- [46] M. Gray and W. Morsi, "Application of wavelet-based classification in nonintrusive load monitoring," in Canadian Conference on Electrical and Computer Engineering (CCECE), Halifax, 2015.
- [47] S. Tabatabaei, S. Dick and W. Xu, "Toward Non-Intrusive Load Monitoring via Multi-Label Classification," IEEE Transactions on Smart Grid, vol. 8, no. 1, pp. 26- 40, 2017.
- [48] J. Gillis, A. S.M. and W. Morsi, "Nonintrusive Load Monitoring Using Wavelet Design and Machine Learning," IEEE Transactions on Smart Grid, vol. 7, no. 1, pp. 320-328, 2015.
- [49] J. Gillis and W. Morsi, "Non-Intrusive Load Monitoring Using Semi-Supervised Machine Learning and Wavelet Design," IEEE Transactions on Smart Grid, vol. 8, no. 6, pp. 2648-2655, 2016.
- [50] S. Mallat and G. Peyre, A Wavelet Tour of Signal Processing : The Sparse Way, Elsevier Science and Technology, 2008.
- [51] H. Lam, G. Fung and W. Lee, "A Novel Method to Construct Taxonomy Electrical Appliances Based on Load Signaturesof," IEEE Transactions on Consumer Electronics, vol. 53, no. 2, pp. 653-660, 2007.
- [52] K. Suzuki, S. Inagaki, T. Suzuki, H. Nakamura and K. Ito, "Nonintrusive appliance load monitoring based on integer programming," in SICE Annual Conference, Tokyo, 2008.

- [53] T. Hassan, F. Javed and N. Arshad, "An Empirical Investigation of V-I Trajectory Based Load Signatures for Non-Intrusive Load Monitoring," *IEEE Transactions on Smart Grid*, vol. 5, no. 2, pp. 870-878, 2014.
- [54] L. Du, D. He, R. Harley and T. Habetler, "Electric Load Classification by Binary Voltage–Current Trajectory Mapping," *IEEE Transactions on Smart Grid*, vol. 7, no. 1, pp. 358-365, 2016.
- [55] T. Huang, W. Wang and K. Lian, "A New Power Signature for Nonintrusive Appliance Load Monitoring," *IEEE Transactions on Smart Grid*, vol. 6, no. 4, pp. 1994-1995, 2015.
- [56] D. Teshome, T. Huang and K. Lian, "Distinctive Load Feature Extraction Based on Fryze's Time-Domain Power Theory," *IEEE Power and Energy Technology Systems Journal*, vol. 3, no. 2, pp. 60-70, 2016.
- [57] J. Gao, E. Kara, S. Giri and M. Berges, "A feasibility study of automated plug-load identification from high-frequency measurements," in *Global Conference on Signal and Information Processing (GlobalSIP)*, Orlando, 2015.
- [58] S. Lin, L. Zhao, F. Li, Q. Liu, D. Li and Y. Fu, "A nonintrusive load identification method for residential applications based on quadratic programming," *Electric Power Systems Research*, vol. 133, no. 1, pp. 241-248, 2016.

- [59] N. Sadeghianpourhamami, J. Ruysinck, D. Deschrijver, T. Dhaene and C. Develder, "Comprehensive feature selection for appliance classification in NILM," *Energy and Buildings*, vol. 151, no. 1, pp. 98-106, 2017.
- [60] J. Liang, N. S.K.K., G. Kendall and J. Cheng, "Load Signature Study—Part I: Basic Concept, Structure, and Methodology," *IEEE Transactions on Power Delivery* , vol. 25, no. 2, pp. 551-560, 2009.
- [61] M. Bhotto, S. Makonin and I. Bajic, "Load Disaggregation Based on Aided Linear Integer Programming," *IEEE Transactions on Circuits and Systems II: Express Briefs* , vol. 64, no. 7, pp. 792-796, 2016.
- [62] J. Kolter and M. Johnson, "REDD: A public data set for energy disaggregation research," in *Workshop on Data Mining Applications*, 2011.
- [63] M. Aiad and P. Lee, "Unsupervised approach for load disaggregation with devices interactions," *Energy and Buildings*, vol. 116, no. 1, pp. 96-103, 2016.
- [64] G. Koutitas and L. Tassiulas, "Low Cost Disaggregation of Smart Meter Sensor Data," *IEEE Sensors Journal*, vol. 16, no. 6, pp. 1665-1673, 2016.
- [65] M. Durling, Z. Ren, N. Visnevski and L. Ray, "Cognitive electric power meter". US Patent 7693670, 2010.
- [66] S. Makonin, F. Popowich and B. Gill, "The cognitive power meter: Looking beyond the smart meter," in *IEEE Canadian Conference on Electrical and Computer Engineering (CCECE)*, Regina, 2013.

- [67] P. Ribeiro, *Power Systems Signal Processing for Smart Grids*, Wiley, 2014.
- [68] S. Gupta, M. Reynolds and S. Patel, "ElectriSense: single-point sensing using EMI for electrical event detection and classification in the home," in *Proceedings of the 12th ACM international conference on Ubiquitous computing*, Copenhagen, 2010.
- [69] A. Martino, A. Ghiglietti, F. Ieva and A. Paganoni, "A k-means procedure based on a Mahalanobis type distance for clustering multivariate functional data," *Statistical Methods & Applications*, vol. 28, no. 2, pp. 301-322, 2019.
- [70] W. Li, A. Monti and F. Ponci, "Fault Detection and Classification in Medium Voltage DC Shipboard Power Systems With Wavelets and Artificial Neural Networks," *IEEE Transactions on Instrumentation and Measurement*, vol. 63, no. 11, pp. 2651-2665, 2014.
- [71] O. Hamid, M. Barbosou, P. Papageorgas, K. Prekas and C. Salame, "Automatic recognition of electric loads analyzing the characteristic parameters of the consumed electric power through a Non-Intrusive Monitoring methodology," *Energy Procedia*, vol. 119, no. 1, pp. 742-751, 2017.
- [72] T. Sainath, O. Vinyals, A. Senior and H. Sak, "Convolutional, Long Short-Term Memory, fully connected Deep Neural Networks," in *IEEE International*

Conference on Acoustics, Speech and Signal Processing (ICASSP), Brisbane, 2015.

[73] J. Zhang and C. Zong, "Deep neural networks in machine translation: an overview.(Natural Language Processing)(Report)," IEEE Intelligent Systems, vol. 30, no. 5, pp. 16-25, 2015.

[74] S. Saadatnejad, M. Oveisi and M. Hashemi, "LSTM-Based ECG Classification for Continuous Monitoring on Personal Wearable Devices," IEEE Journal of Biomedical and Health Informatics, vol. Early Access, pp. 1-9, 2019.

[75] H. Huynh, L. Dang and D. Duong, "A New Model for Stock Price Movements Prediction Using Deep Neural Network," in Proceedings of the Eighth International Symposium on information and communication technology, 2017.

[76] P. Murthy, J. Amarnath, S. Kamakshiah and B. Singh, "Wavelet Transform Approach for Detection and Location of Faults in HVDC System," in IEEE Region 10 and the Third international Conference on Industrial and Information Systems, Kharagpur, 2008.

[77] A. Abdollahi and S. Seyedtabaai, "Comparison of Fourier & Wavelet Transform Methods for Transmission Line Fault Classification," in

International Power Engineering and Optimization Conference (PEOCO), Shah Alam, 2010.

[78] J. G. W. Ning, "A wavelet-based method to extract frequency feature for power system fault/event analysis," in IEEE Power & Energy Society General Meeting, Calgary, 2009.

[79] A. Maqsood, N. Rossi, Y. Ma, K. Corzine, L. Parsa and D. Oslebo, "STFT-Based Event Detection and Classification for a DC Pulsed Load," 2019 IEEE Electric Ship Technologies Symposium (ESTS), 2019, pp. 492-498.

[80] Q. Xiong, X. Liu, X. Feng, A. Gattozzi, Y. Shi, L. Zhu, J. Shengchang and R. Hebner, "Arc Fault Detection and Localization in Photovoltaic Systems Using Feature Distribution Maps of Parallel Capacitor Currents," IEEE Journal of Photovoltaics, vol. 8, no. 4, pp. 1090-1097, 2018.

[81] Q. Xiong, X. Feng, A. Gattozzi, X. Liu, L. Zheng, L. Zhu, J. Shengchang and R. Hebner, "Series Arc Fault Detection and Localization in DC Distribution System," IEEE Transactions on Instrumentation and Measurement , vol. Early Access, pp. 1- 13, 2019.

[82] L. Herrera and X. Yao, "Parameter Identification Approach to Series DC Arc Fault Detection and Localization," in IEEE Energy Conversion Congress and Exposition (ECCE), Portland, 2018.

- [83] L. Yue, V. Le, Z. Yang and X. Yao, "A Novel Series Arc Fault Detection Method using Sparks in DC Microgrids with Buck Converter Interface," in IEEE Energy Conversion Congress and Exposition (ECCE), Portland, 2018.
- [84] A. Maqsood, N. Rossi, Y. Ma, K. Corzine, L. Parsa and D. Oslebo, "A Coupled-Inductor Dc Breaker with STFT-Based Arc Detection," 2020 IEEE Applied Power Electronics Conference and Exposition (APEC), 2020, pp. 1747-1754.
- [85] J. Stevens, Robust model-based fault diagnosis [sic] for a DC zonal electrical distribution system, Monterey: NPS PhD Thesis, 2007. [86] E. Calderon-Mendoza, P. Schweitzer and S. Weber, "Kalman filter and a fuzzy logic processor for series arcing fault detection in a home," International Journal of Electric Power and Energy Systems, vol. 107, no. 1, pp. 251-263, 2019.
- [87] A. Nanduri and L. Sherry, " Anomaly detection in aircraft data using Recurrent Neural Networks (RNN)," in Integrated Communications Navigation and Surveillance (ICNS), 2016.
- [88] T. de Bruin, K. Verbert and R. Babuska, "Railway Track Circuit Fault Diagnosis Using Recurrent Neural Networks," IEEE Transactions on Neural Networks and Learning Systems, vol. 28, no. 3, pp. 523-533, 2017.

- [89] M. Cheng, Q. Li, J. Lv, W. Liu and J. Wang, "Multi-Scale LSTM Model for BGP Anomaly Classification," *IEEE Transactions on Services Computing*, vol. Early Access, pp. 1-14, 2018.
- [90] H. Habler and A. Shabtai, "Using LSTM encoder-decoder algorithm for detecting anomalous ADS-B messages," *Computers and Security*, vol. 78, no. 1, pp. 155-173, 2018.
- [91] P. Malhotra, A. Ramakrishnan, G. Anand, L. Vig, P. Agarwal and G. Shroff, "LSTM-based Encoder-Decoder for Multi-sensor Anomaly Detection," *ArXiv*, 2016.
- [92] D. Park, Y. Hoshi and C. Kemp, "A Multimodal Anomaly Detector for Robot Assisted Feeding Using an LSTM-Based Variational Autoencoder," *IEEE Robotics and Automation Letters*, vol. 3, no. 3, pp. 1544-1551, 2018.
- [93] A. Maqsood, D. Oslebo, K. Corzine, L. Parsa and Y. Ma, "STFT Cluster Analysis for DC Pulsed Load Monitoring and Fault Detection on Naval Shipboard Power Systems," in *IEEE Transactions on Transportation Electrification*, vol. 6, no. 2, pp. 821-831, June 2020.
- [94] L. Posam, Y. Ma, K. Corzine, "Dc Fault Detection of Naval Shipboard Pulsed Power Loads Using Logistic Regression" 2022 IEEE Applied Power Electronics Conference and Exposition (APEC), 2022, pp. 2040-2043.

- [95] Y. Ma, D. Oslebo, A. Maqsood and K. Corzine, "Pulsed-Power Load Monitoring for an All-Electric Ship: Utilizing the Fourier Transform Data-Driven Deep Learning Approach," in *IEEE Electrification Magazine*, vol. 9, no. 1, pp. 25-35, March 2021.
- [96] Y. Ma, D. Oslebo, A. Maqsood and K. Corzine, "DC Fault Detection and Pulsed Load Monitoring Using Wavelet Transform-Fed LSTM Autoencoders," in *IEEE Journal of Emerging and Selected Topics in Power Electronics*, vol. 9, no. 6, pp. 7078-7087, Dec. 2021.
- [97] Y. Ma, A. Maqsood, K. Corzine and D. Oslebo, "Long Short-Term Memory Autoencoder Neural Networks Based DC Pulsed Load Monitoring Using Short-Time Fourier Transform Feature Extraction," 2020 IEEE 29th International Symposium on Industrial Electronics (ISIE), 2020, pp. 912-917.
- [98] Y. Ma, A. Maqsood, D. Oslebo and K. Corzine, "Wavelet Transform Data-Driven Machine Learning-Based Real-Time Fault Detection for Naval DC Pulsating Loads," in *IEEE Transactions on Transportation Electrification*, vol. 8, no. 2, pp. 1956-1965, June 2022.
- [99] Y. Ma, A. Maqsood, D. Oslebo and K. Corzine, "Real-time Dc Pulsed Power Load Monitoring using Simplified k-NN Algorithms," 2021 IEEE Energy Conversion Congress and Exposition (ECCE), 2021, pp. 1334-1338.

- [100] Y. Ma, A. Maqsood, D. Oslebo and K. Corzine, "Comparative Analysis of Data Driven Fault Detection using Wavelet and Fourier Transform for Dc Pulsed Power Load in the All-Electric Ship," 2021 IEEE Applied Power Electronics Conference and Exposition (APEC), 2021, pp. 1343-1347.
- [101] Y. Ma, A. Maqsood, D. Oslebo and K. Corzine, "Real-time Cluster Analysis based Fault Detection for Dc Pulsed Power Load in the All-Electric Ship," 2021 IEEE Applied Power Electronics Conference and Exposition (APEC), 2021, pp. 2748-2752.
- [102] J. Teslade, "DWT Filter Bank," [Online]. Available: https://commons.wikimedia.org/wiki/File:Wavelets_-_Filter_Bank.png, 2005.
- [103] J. Teslade, "SWT Implementation," [Online]. Available: https://en.wikipedia.org/wiki/Stationary_wavelet_transform#/media/File:Wavelets_-_SWT_Filter_Bank.png, 2005.
- [104] D. Wang, L. Zhang and A. Vincent, "Recursive wavelet filters for video coding," Proceedings of SPIE, vol. 5960, no. 1, pp. 653-660, 2005.